Published in final edited form as:
Biomater Sci. 2014 April 1; 2(4): 436–471. doi:10.1039/C3BM60181A.

BIOPHYSICAL PROPERTIES OF NUCLEIC ACIDS AT SURFACES RELEVANT TO MICROARRAY PERFORMANCE

Archana N. Rao[1] and **David W. Grainger**[1,2,*]

[1]Department of Pharmaceutics and Pharmaceutical Chemistry, University of Utah, Salt Lake City, UT 84112 USA

[2]Department of Bioengineering, University of Utah, Salt Lake City, UT 84112 USA

Abstract

Both clinical and analytical metrics produced by microarray-based assay technology have recognized problems in reproducibility, reliability and analytical sensitivity. These issues are often attributed to poor understanding and control of nucleic acid behaviors and properties at solid-liquid interfaces. Nucleic acid hybridization, central to DNA and RNA microarray formats, depends on the properties and behaviors of single strand (ss) nucleic acids (e.g., probe oligomeric DNA) bound to surfaces. ssDNA's persistence length, radius of gyration, electrostatics, conformations on different surfaces and under various assay conditions, its chain flexibility and curvature, charging effects in ionic solutions, and fluorescent labeling all influence its physical chemistry and hybridization under assay conditions. Nucleic acid (e.g., both RNA and DNA) target interactions with immobilized ssDNA strands are highly impacted by these biophysical states. Furthermore, the kinetics, thermodynamics, and enthalpic and entropic contributions to DNA hybridization reflect global probe/target structures and interaction dynamics. Here we review several biophysical issues relevant to oligomeric nucleic acid molecular behaviors at surfaces and their influences on duplex formation that influence microarray assay performance. Correlation of biophysical aspects of single and double-stranded nucleic acids with their complexes in bulk solution is common. Such analysis at surfaces is not commonly reported, despite its importance to microarray assays. We seek to provide further insight into nucleic acid-surface challenges facing microarray diagnostic formats that have hindered their clinical adoption and compromise their research quality and value as genomics tools.

Keywords

DNA; microarray assay; diagnostics; ssDNA; dsDNA; hybridization; tethered chain; polyelectrolyte; mushroom regime; brush regime; DNA conformation; persistence length; radius of gyration; thermodynamics; kinetics; spacer; diluents; molecular beacons; Coulombic blockage; printed spot heterogeneity; Marangoni; coffee ring; fluorescent signal intensity

[*]to whom correspondence should be addressed: David W. Grainger, david.grainger@utah.edu.

1. Introduction

Nucleic acid microarray technology enables gene expression profiling for thousands of genes in parallel in a single assay.[1] Information from DNA microarray-based assays is used in genotyping,[2] DNA–protein interactions[3], genome sequencing,[4] pharmacogenomics and drug discovery[5], infectious and genetic disease[6], cancer diagnostics[7], forensic and genetic identification[8], toxicology[9] and many other applications. Though a powerful high-throughput tool with assorted applications, microarray analytical accuracy and assay reliability in assessing clinical samples, producing analyte quantitation and in clinical decision-making is questionable.[10] Data analysis and interpretation have provided unique challenges and “the transition from bedside to bench to bedside” has been slower than expected due to various pitfalls in using its diagnostic and prognostic insights.[11] Despite common perceptions otherwise, only four FDA-approved microarray based diagnostics are currently marketed for clinical decision guidance.[12] Requirements for assay standardization and validation for each microarray experimental step, emphasizing quality control protocols in array fabrication, scanner calibration and data verification, have proven difficult to surmount. The USA FDA’s initiative of Microarray Quality Control I, II and III (MAQC) consortia are charged with identifying and assessing critical factors affecting array data quality, and to optimize and standardize microarray assay and analytical procedures.[13] This effort has focused on resolving procedural discrepancies and improving assay and data repeatability and reproducibility among various array platforms, but has not yet effectively addressed several fundamental root causes of assay variability issues.[14, 15]

Despite the various dimensions to this assay problem, at their basis commonly lies the understanding of biophysical aspects of short single-strand nucleic acids as surface-immobilized probes, and their resulting behavior at surfaces in producing hybridization with target analytes. Certainly improved bioinformatics and biostatistics for assessing target capture data and accurate signal interpretation remain critical to yielding meaningful, relevant medical outcomes.[16–18] Nonetheless, a first-principles perspective of DNA properties at surfaces and its central control of the molecular interactions controlling these data is important to guide array fabrication and assay design. Table 1 summarizes some major obstacles facing the successful design of improved DNA microarrays. Many of these challenges rely on a basic understanding and ability to exert some control over the molecular “disposition” of single ssDNA strands immobilized on assay surfaces to promote target binding – on various commercial surfaces, different printing milieus, drying conditions, hybridization buffers and assay compositions.

Recent technological advances, new analytical methods and sophisticated experimental tools such as optical (e.g., fluorescence methods), surface analytical and molecular force approaches have yielded new information on the dynamic behaviors and properties of nucleic acids, both in bulk states and on surfaces. Parameters regarding ssDNA molecular conformations, structural transitions and dynamics at nanometer scales and in short (i.e., millisecond) time frames, provide data for ssDNA relevant to understanding certain behaviors on microchips and array surfaces. Additionally, new in silico computational models, molecular dynamics simulations, and software tools have produced correlations

with experimental data as well as accuracy in predicting certain ssDNA structural phenomena. While simulations and modeling are recognized to have some discrepancies with experimental data, they should now be more capable of providing valuable insight into understanding certain, relevant biophysical properties.[19]

2. Microarray design and fabrication

The nucleic acid microarray strategy exploits surface-tethered complementary oligonucleotides on solid supports -- often dense-packed, surface-grafted, immobilized, adsorbed or printed short nucleotide ensembles -- to capture targeted complementary nucleotides from a sample via hybridization. Figure 1 shows general schematics for the working principles behind the DNA microarray design. Synthetic ssDNA assay probes are typically short (i.e., usually 20–70, up to 200 bases). Probe immobilization at a solid-liquid interface, typically involving droplet printing and subsequent rapid evaporation at a solid-air interface, produces a unique dried tethered state for ssDNA not found naturally. These unconventional immobilization and processing steps with an unusual synthetic ssDNA construct, and resulting ssDNA surface microenvironments, all profoundly influence subsequent ssDNA-surface interactions and dsDNA hybridization responses with incoming ssDNA or RNA targets. Therefore, understanding both ss- and dsDNA interfacial behavior during this processing is critical to asserting control over assay performance and in designing rational steps for improvements that address the certain needs described in Table 1.

Various strategies are used for realizing DNA microarray constructions shown in Figure 2, with several ssDNA-surface immobilization methods on a wide range of solid (and often poorly defined) substrate chemistries and forms.[20, 21] ssDNA probe immobilization on a surface has three fundamental approaches broadly characterized as: 1) ssDNA “grafting to”; 2) ssDNA “grafting from”; and 3) ssDNA nanodroplet printing/drying. In the first approach, anionic polyphosphate ssDNA probe oligomers are either adsorbed to cationic surfaces electrostatically, or by combinations of polar and hydrophobic interfacial interactions to other surfaces (i.e., nitrocellulose, silicon oxide, or polypropylene). In the second “grafting from” approach, fluidics, photolithography and photochemistry are combined with automated microprocessing to sequentially add and spatially direct each individual DNA nucleotide to grow ssDNA probe chains directly from chemical primer sites, pre-immobilized across patterned surfaces. In the third strategy, automated dispensing equipment places ssDNA probe solution droplets in specified surface locations and allows rapid drying by evaporation, effectively adsorbing the dried ssDNA probes to specific locations as disorganized ssDNA surface films. These approaches are summarized in Figure 2. Importantly, each method yields different, physically distinct endpoints for resulting DNA probes on the surface. These fundamental DNA-substrate fabrication differences then result in distinct capabilities for probe-target interactions and assay hybridization yields and signals.

Commercially popular amine-terminated organosilane-coated and poly(L-lysine)-modified glass slides provide cationic surfaces for electrostatically binding anionic ssDNA probes, the basis for several popular microarray products using the “grafting to” approach (see Figure

2A).[22, 23] Alternatively, covalent “grafting to” approaches for DNA probes are diverse, but many use terminally amine-modified ssDNA and amine-reactive surface chemistries, including aldehyde, isothiocyanate, isocyanate chemistry and also reactive esters including *p*-nitro- and perfluoro-phenyl and N-hydroxysuccinimide (NHS) terminal groups on coated slides.[24] “Grafting from” strategies are also commercially used in ssDNA array fabrication. For example, Affymetrix combines masked-based automated photolithography and combinatorial chemistry to synthesize very high density DNA chips.[25] Hydroxylated, silanized fused silica wafers are derivatized with a linker molecule and a light-sensitive protecting group. Photolithographic masks then illuminate specific locations on the silanized wafer, with UV exposure causing chemical site deprotection to activate surface chemistry that then couples free nucleotides onto the silica wafer only where irradiated (Figure 2B).[26] Additional capping steps then prevent unattached molecules from becoming probes. Nucleotide side chains are also protected to prevent branched-chain formation. Photo-induced deprotection, coupling and capping steps are sequentially at multiple sites under computer-controlled mask pattern changes, and continued until full-length immobilized probes of diverse sequence variation are fabricated on chip at known sites, controlled at high density.[27] In an alternative commercial approach, NimbleGen (Roche) builds arrays using photo-deposition chemistry based on a mask-less array synthesizer (MAS), specifically a mask-less light projector acting as a ‘virtual mask’ instead of the physical photomasks used by Affymetrix.[28] In each case, the stepwise photo-controlled on-chip synthesis yield is approximately 85–95% hence oligonucleotide probes longer than 25 bases are not reliably synthesized with high fidelity. Alternatively, patterned metal films facilitate patterned DNA islands as chemisorbed DNA adlayers from solution.[29] Figure 2C shows thiolated DNA probes that react spontaneously with clean, patterned gold, copper, platinum, and silver metallic surfaces via metal-thiolate bond formation from aqueous solution to yield immobilized DNA probes with patterned array fidelity corresponding to metal patterns. This popular solution-based metal-thiolate coupling chemistry has been widely studied as a fundamental method for accessing DNA single-point attached monolayer films as well as commercialized for array and assay uses.[30, 31]

Figure 2D depicts more common DNA microarray fabrication using direct droplet printing and evaporation based on high definition spatial deposition of nanoliter probe solution volumes. Dispensing of these droplets can exploit contact precision pins, inkjets, bubble jets or piezo-actuated technologies capable of reliably dispensing 100 pL to 2 mL volumes per array area. Contact pin printing usually results in spot densities of 2000–4000 spots/cm^2 of ~100 micron spot diameters, while non-contact (i.e., piezo) printing yields slightly higher spot density with smaller spot diameters. Reliable fabrication of printed probe microspotted arrays is a multi-parameter optimization challenge. Spot performance in hybridization assay is a function of final probe spot morphology and probe density, and probe lateral distribution within the spots affects target hybridized density and resulting target signal distribution.[32–34] Little methods standardization is currently present, meaning that each spotting recipe, instrument, surface and print protocol produces different DNA probe spot properties with different final dried densities and resulting distinct probe/target hybridization capabilities, therefore different assay signals. This issue is central to the variable metrics challenges behind current DNA array-based assay answers.

3. Immobilized DNA-surface models

Given these diverse DNA array fabrication methods, all but droplet spotting methods are expected to yield immobilized monolayers of probe nucleic acids on supports. Droplets dry rapidly *in situ*, leaving behind a thick dried residue of ssDNA and buffer salts that may or may not be rinsed away in subsequent washing steps to yield reliable DNA immobilized thin films. This leads to high density and random orienting ssDNA probes on surfaces. Additionally, microarray “grafting to” immobilization methods (e.g., Figures 2A, C, D) all use pre-synthesized oligonucleotide probes purified by capillary electrophoresis or high-performance liquid chromatography prior to array deposition of nearly homogeneous probe samples, increasing assay specificity. By contrast, *in situ* probe synthesis (Figure 2B) is not 100% accurate, and ready validation of the fidelity of the final ssDNA probe composition on the array surface is difficult.[35] These photo-generated “grafting from” microarrays therefore contain significant nucleotide chain defects distinct from the desired sequence.[36] A consequence of high probe density is slow hybridization kinetics that produces incomplete duplexing in practical assay timelines, resulting in low hybridization efficiencies and reduced hybridized target analyte capture and sensitivity. In contrast, low surface probe densities lead to relatively fast kinetics but with absolute hybridized target signal limited by the reduced surface probe amounts.[37] This trade-off between signal yield and assay speed is also a central issue for such printed array formats. Table 2 summarizes array spot areas and probe densities for the various immobilization methods.[29, 38, 39] A “Goldilocks principle” might be appropriately assigned to the current state of ssDNA tethering and density at surfaces in search of the optimal signal generation by target capture. This is depicted in Figure 3. High density of immobilized probe presents steric and electrostatic barriers (detailed below) that preclude accurate target capture and alter hybridization kinetics (Figure 3A). Low probe densities capture target at high efficiency but the end result is insufficient signal and high background noise from non-specific capture (Figure 3B). Optimal probe density, while such optimization is case dependent on probe sequence and length and surface assay conditions, might be described as a condition between these two extremes where sufficient signal is produced at reasonable time scales and with fidelity to target abundance and sequence (Figure 3C). Only thorough understanding of both ssDNA and resulting dsDNA chain duplexing behavior and properties at surfaces will permit rational designs for such optimization.

Knowledge and control of ssDNA probe density and its physical state are fundamentally important to interpreting differences in assay signal from both label-free and labeled microarray assays, and to design more highly efficient, reproducible assay formats. Importantly, each ssDNA probe immobilization approach yields distinctly different probe molecular fates that determine the resulting dsDNA duplex events on surfaces. For example, physi- or chemi-sorption of oligo-ssDNA probe chains to surfaces in the “grafting to” approach (Figure 2A) provide little control over immobilized ssDNA chain densities and probe chain segmental conformations. In these cases, relative amounts of surface ssDNA probe chain loops, trains, and tails (see Figure 4)[40, 41] are stochastic endpoints of the adsorption process and drying, with distances between adsorbed chains unknown, uncontrolled and perhaps entangled, affecting pairing with incoming targets. A critical

physicochemical distinction from other ssDNA probe immobilization methods is the largely unproven presumption that such adsorbed ssDNA chains (i.e., not single point attached) lie largely horizontal on the surface due to the multiplicity of chain-surface adsorption sites and polyvalent DNA chain segments.

By contrast, end-point ssDNA immobilization resulting from both photochemical *in situ* patterning/reaction approaches, as well as metal-thiolate probe chemisorption and covalent chain-end reaction chemistry (Figure 4B,C), is presumed to produce brush-like chain conformations oriented largely orthogonal to the surface.[42–44] These important differences in immobilized probe ssDNA chain orientations as a function of fabrication method should be reflected in their resulting kinetics, thermodynamics and efficiencies of target capture during duplex formation under assay conditions.

These influences can be appreciated by inspection of idealized DNA chain physical states on surfaces, shown in Figure 4. Uncontrolled ssDNA-surface interactions yield adsorbed DNA chains with multiple surface-binding states, leading to the classic surface-immobilized polymer “loop-trains-tails” surface configurational scenario (Figure 4A).[45] How DNA-DNA duplexes form from this random surface-adsorbed state in microarray assays, given that short ssDNA probe oligomers of 20–30 bases require substantial complementary pairing to form stable duplexes with targets, is not known. Yet, many long-standing nucleotide array platforms utilize this ssDNA probe (physi-)adsorption approach (e.g., FAST™ slides) to create arrays.[46, 47] End-point grafted probes (Figure 4B, e.g., Affymetrix or Nimblegen arrays) produce distinctly different immobilized probe states where ssDNA chain lateral density in brush-like formats is a function of the chain’s size and other physical conditions. How this chain physical state is understood for ssDNA immobilized on array surfaces determines how we understand its interactions with complementary and non-complementary ssDNA targets it encounters, how it can select perfect duplex partners to achieve reliable assay and how microarray assays might be better designed to reliably achieve this endpoint.

4. Idealized tethered polymer chain models

Fortunately, immobilized chain polymer physics has experienced considerable theoretical model development and validation using several experimental immobilized chain models. These tethered chain systems exploit polymer statistical conformational and configurational properties derived from their bulk solution states. In bulk dilute solution, generic polymer size is idealized by the Flory radius, R_F, the end-to-end distance for an ideal but expanded chain where self-avoiding random walks and excluded volume effects from chain expansion dominate. This condition is distinct from ideal chains defined as having freely jointed chains and conformational random walks, comprising monomers as rigid rods of fixed length and chain orientation completely independent of the orientations and positions of neighboring monomers, to the extent that two monomers can co-exist at the same place (i.e., phantom chain). Polymer R_F scales with the square root of the polymer’s end-to-end distance, $<R>$ (i.e., $R_F = <R^2>^{0.5}$). By contrast, the chain’s radius of gyration, R_g, is substantially smaller than the polymer’s end-end distance in the freely jointed chain model, so that $R_g^2 = R_F^2/6$. Additionally, Flory’s mean-field model polymer size yields a well-known scaling law for R_g as $R_g \sim N^{\nu}$, where N is the number of bonded polymer segments (i.e., degree of

polymerization). Chains in good solvents yield values for the Flory exponent ν as $\nu = 3/5$ (expanded), and for bad solvents as $\nu = 1/3$ (condensed).[48] In so-called theta conditions, $\nu = 1/2$, the result consistent with the simple random walk model, so that this chain behaves ideally.[49] Generally, then the Flory expression for R_g is:

$$R_g \alpha N^{\nu} b \quad (1)$$

where N^{ν} is the number of DNA nucleotides, b is the size of the nucleotide, and ν reflects the quality of solvent (i.e., salt concentration).

In 1977, Alexander extended polymer scaling concepts to strongly stretched, densely grafted polymer chains on impenetrable surfaces (termed polymer brushes). This was then further improved by de Gennes using a blob modification to the tethered idealized chain scaling model. The resulting Alexander-de Gennes scaling model for polymers end-grafted to surfaces, and resulting properties and possible applications is widely accepted due to its simplicity and usually good “real chain” approximations of ideal ‘bulk” solvent-swollen brush properties such as brush height and brush modulus.[50] Schematic depictions for idealized tethered “mushroom” and “brush” polymer structures on substrates are idealized in Figure 4B. In the “mushroom” regime, immobilized chains are considered to occupy hemispherical volumes separated by distances precluding lateral chain-chain overlap. de Gennes demonstrated that the mushroom regime reflects the lower limit of chain immobilized density (σ) where chains do not overlap at a lateral surface spacing distance, D. Ideal chain separations of $R_g < D$ lead to a tethered polymer surface density, $\sigma < N^{-6/5}$, meaning that surface chain density is nearly inversely proportional to polymer length. When σ increases to $\sigma > N^{-6/5}$, grafted chains begin to crowd each other, with conformational extensions away normal from the surface to reduce segment crowding and repulsive entropic, enthalpic and possible polar or electrostatic issues, yielding a “brush” of extended chains.[51] The basic enduring relationship for ideal polymer brushes is the power scaling law relation between swollen brush thickness, H, and polymer grafting density, σ, where $H \sim \sigma^{\nu}$.[52] The Flory scaling exponent abruptly changes from $\nu = 0$ to $\nu = 1/3$ when grafted, ideal polymer chain spacing becomes less than R_g (i.e., the so-called mushroom-to-brush density transition).

A critical primary assumption in the Alexander-de Gennes polymer brush model is that monomer density is assumed to be constant throughout the brush. This implies that the tethered polymers are uniformly stretched, all chain ends are located at the outer edge of the brush.[53] This oversimplification underestimates the conformational entropy of the grafted chains. More than 30 years of efforts have sought to describe the polymer brush theory experimentally and theoretically with the model by incorporating different grafting scenarios such as graft density, chain length, good or bad solvents (i.e., differential chain swelling), charged polymer chains, aqueous solvents of varying ionic strengths, presence of bulk surfactants and colloids, and many other variables. Experimental alignment, given these experimental complexities, with the original Alexander-de Gennes theory has been difficult. This has prompted evolution of newer scaling theories, analytical self-consistent-field (aSCF) models and other numerical models to improve theoretical accuracy.[50, 54, 55]

The aSCF model assumes that grafting density is sufficiently high for the brush to be laterally homogeneous, implying that both monomer and chain end density are solely functions of distance from the impenetrable grafting surface. A parabolic density distribution profile is predicted in the brush compared to the constant “box-model” of Alexender-de Gennes model. The numerical self-consistent-field (nSCF) models overcomes the limitations of aSCF,[56] modeling monomer density in the brush at a given distance from the grafting plane as the combined sum of the density “σ” at the given distance “H” of all possible conformations, weighted by the probability of each conformation.[57] The equilibrium density distribution, self-consistent with the distribution of polymer conformations it generates, is determined numerically for a given grafting density, chain length, adsorption properties and solvent conditions. This nSCF model accommodates long chains at relatively high grafting densities under good solvent conditions. Also, a segment depletion region close to the surface is predicted, as the grafting plane impermeability is entropically unfavored.[58] The most important limitation is the assumption of most probable chain conformation and fluctuations around this conformation are not considered. This is especially limiting for low grafting densities or short chains. aSCF and nSCF are applicable to long chains grafted at either a low grafting density (mushrooms) or at a high grafting density (brushes).

Nonetheless, very recent work [59] does show that single-strand tethered DNA of ~1000 bases does follow brush scaling predictions for polyelectrolyte brush height [60] as a function of both chain density and ionic strength. So, to a certain extent, intermediate length polyelectrolyte brush behaviors in high ionic strength milieu can be predicted. A large number of experimental tethered chain systems (i.e., most DNA brush systems among them) will not meet these criteria, however, either due to far shorter chains (e.g., 20–80 bases) or an insufficient grafting density to obtain a polymer brush, and hence termed as quasi-static or pseudo-static regimes.[61] Additionally, it is important to note that the exact chain conformation for grafted layers depends on the grafting density and solvent conditions. The above models are limited to good solvent; the Scheutjens–Fleer self-consistent field lattice model (SF-SCF) is used for chain grafts in bad solvents.[62]

4.1 Scaling theories and DNA brushes

Polymer scaling models have been applied to tethered polyelectrolyte DNA at surfaces using many theoretical and experimental approaches. ssDNA is often described as a random polymer coil with long-range interactions expected to induce swollen polyelectrolyte configurations characterized by a Flory radius. Distinguishing features of polyelectrolyte brushes result from Coulombic interactions between charged monomers within the chains. These interactions are partially screened, also in salt-free solution, by the presence of mobile counterions, ensuring system electroneutrality. In electrolyte solutions, both co- and counter-ions contribute significantly to this screening. Additionally, immobilized charges present on the tethering surface also elicit long-range attractive or repulsive forces between the surface and grafted chains. Charges exist on experimental surfaces from ions adsorbed from solution, surfactants adsorbed to hydrophobic surfaces, or solid-state functional groups dissociated on the surface. Repulsion of charged polymer segments both from this charged surface and from other charged polymer chain segments results in the extension of grafted

polyions in the direction perpendicular to the surface. Magnitudes of these two repulsive forces determine the brush conformational dynamics in polyelectrolyte brushes. Electro-neutrality overall is derives from the presence of a compensating amount of mobile counterions in the solution. A critical length scale in the system is the Gouy–Chapman double layer thickness (i.e., Debye screening length) determined by the media ionic strength and valencies.

Several models have been proposed to understand the effects of added salt (increased ionic strength) on polyelectrolyte brush height.[63] Zhulina's group [64, 65] adapted theoretical brush models to ssDNA "brushes" at surfaces and the important crossover to the mushroom regime of non-overlapping tethered polyelectrolyte tails, and compare DNA hybridization constants on surfaces versus the bulk [66]. They used a Flory version of the Alexander model for ssDNA brushes as applied to terminally anchored polyelectrolytes in aqueous solutions of high ionic strength, modifying it to incorporate the influence of an impenetrable grafting surface.[51] Dense, strongly ionized polymer brushes produce the so-called "osmotic" regime where the majority of the mobile counterions are trapped within the polyelectrolyte brush to compensate the immobilized polyanion brush charge density. The resulting osmotic pressure from these entrapped counterions swells this strongly charged brush with solvent (water), and the equilibrium balance between this osmotic pressure and chain entropic elastic forces produce a scaling expression for the equilibrium thickness of this "osmotic brush", *H*:

$$H \alpha N m^{-\frac{1}{2}} a \quad (2)$$

where *m* is the number of neutral (uncharged) monomer units in the chain between two neighboring charged monomers and *a* is the monomer unit length (0.3–0.6nm).[67] Eq. 2 shows that a highly charged polyanion brush thickness (H) can be independent of grafting density, σ, under these conditions. Additionally, the "intrinsic" Debye screening length provided by counterions within the brush is much smaller than the osmotic brush thickness, H. This indicates that the brush is electroneutral locally on a length scale larger than the Debye length in this osmotic regime, supporting the local electroneutrality approximation (LEA) applied in the structural analysis of osmotic brushes. This LEA is also important to understand how target ssDNA polyanions approach and penetrate immobilized ssDNA probes to form duplexes on array surfaces in high ionic strength conditions used for hybridization experiments.

By contrast, weak polyelectrolyte brushes comprising anchored polymer chains establish a local equilibrium between neutral, undissociated and charged, dissociated polymer moieties. In such systems, the degree of dissociation depends on the local pH value and local charge density, also considering added salt. A weaker polyanion (less completely charged) brush exhibits brush height increases with increasing salt concentration, described by a scaling function more weakly dependent on grafting density and ionic strength:[68–70]

$$H \alpha N a c_s^{\frac{-1}{3}} \sigma^{\frac{1}{3}} \quad (3)$$

where c_s is the monovalent salt concentration, and σ is anchored polymer chain density. This scaling dependence has recently been further refined to a number of distinct “salting in” brush thickness regimes dependent upon added salt with several different power law dependences.[60] Increasing counterion valency condenses ssDNA more readily to reduce ssDNA charge, facilitating polymer condensation.[71] This long-standing counterion valence-polyion condensation relationship was recently validated also for longer (968 bases) ssDNA brushes.[59] Because bulk phase soluble cations can be exchanged with polyanion brush-associated protons without violating charge neutrality, the degree of brush anion dissociation per polymer chains changes, sometimes yielding polymer brush salts that dissociate more freely than native weak acids with increasing added salt. At lower ionic strength, brush height increases, while at higher ionic strength, weaker polyion brushes have reduced thicknesses similar to strongly charged brushes. Additionally, reduced ionic strength is predicted to stiffen immobilized chains via repulsive ionic interactions on neighboring ssDNA chains. This, however, was not observed experimentally and explained by claiming that the DNA brush attracts a minimal concentration of ions of approx. 1 mM, limiting expected chain electrostatic stiffening.[59] Lastly, the addition of ssDNA oligomeric, polyanion soluble targets outside the brush can elicit a Donnan equilibrium for dense brushes. The immobilized, charged ssDNA probe layer is permeable to small ions to preserve electroneutrality, but not necessarily also to the incoming ssDNA targets as larger macro-scale polyions. The difference in the resulting electrostatic potential from unequal distribution of the large ions influences the distribution of small ions to also be asymmetric across the brush boundary, resulting in global electroneutrality but dissimilar chemical potentials for each ionic species across the brush boundary (layer thickness).[72]

4.2 DNA brushes, hybridization models and intrinsic limitations

Gong and Levicky applied the Halperin Buhot and Zhulina polymer brush theory (HBZ) [51] to understand DNA hybridization isotherms, and the cooperative relationship between probe coverage and ionic strength for the initial hybridization reaction onset and the more complex regimes with increased target binding.[73] Hagan and Chakraborthy predicted hybridization kinetic regimes for surface-tethered ssDNA oligomers with solubilized targets with both theoretical and experimental approach.[74] Their theoretical approach included modifying the Alexander-de Gennes theory combined with the Zimms model of penetrating diffusion for duplexing target. Both experimental and theoretical evidence revealed that nucleation sites near the grafted ends of the polyanion probes are the least accessible; thus, ssDNA targets that preferentially bind to this region show more drastic rate reductions than those that bind near probe free ends. Brush regimes in ssDNA and dsDNA layers were distinguished by Halperin et al. by specifying unique molecular length scales for ssDNA versus dsDNA across a range of parameters: in contrast to the ssDNA random coil, dsDNA is a stiffer rod-like molecule with each base-pair contributing 0.34 nm to its length.[51] The radius of a dsDNA helix is 0.95nm and its cross-sectional area is 28.4 nm^2, given the typical nucleotide monomer size of 0.6nm.

However, two important physicochemical distinctions characteristic of ssDNA immobilized in the various array formats limit applicability of classic polymer chain scaling theories to its analysis. Critically, DNA is a polyanion with high chain charge density and, in array states,

often immobilized as short chain single-strand oligomers (20–60 bases long). Immobilized chain physics models do not frequently address these two conditions (i.e., incompatible with accommodating both hlgh charges and short stiff chain lengths) and at an impenetrable interface. The commonly invoked Gaussian chain elasticity model cannot detail the local structure of the immobilized chain and therefore is mostly applicable to study flexible chains on large length scales where the local chain correlations are negligible. Typical tethered ssDNA array probes of 20–200 bases in water or low ionic strength conditions are often considered short, stiff, rod-like molecules with few degrees of freedom. Persistence length arguments (*vida infra*) support this. However, high ionic strength conditions for hybridization can seemingly allow longer ssDNA molecules to obey scaling relationships.

For example, the Flory and Alexander-de Gennes models for other tethered polymers are compromised for polyelectrolytes: each ssDNA immobilized layer is characterized by distinct ssDNA segmental density distributions normal to the surface (using Gaussian statistics), with the resulting ssDNA layer thickness, H, that produces significant steric and electrostatic barriers to target hybridization.[51] These distributions and thicknesses are highly dependent on chain-chain, chain-surface and chain-solvent electrostatic interactions, without a unifying theory that accurately accounts for all of these factors. The worm-like chain (WLC) model (also called the Kratky-Porod model) is a special case of the freely rotating chain model for very small values of bond angles. This is a good model for stiff polymers, (e.g., dsDNA) for which the flexibility is due to fluctuation of the contour of the chain from a straight line. Recent work has shown as well that for 1000 bases long ssDNA grafted in the mushroom regime[59] the observed sub-linear dependence of height with contour length at high salt (i.e., 250 mM) fits well with the end-to-end distance of a semiflexible polymer in solution (WLC model, i.e., $H \propto R_{WLC}$), showing stiff rod-like behavior for short ssDNA polymers and ideal chain behavior for long ssDNA polymers. Low-density ssDNA probe immobilization (i.e., sometimes below the limit where the ionic double layer Debye length is smaller than the brush thickness, H, and therefore the screening length extends beyond the brush thickness in low salt concentrations) can also facilitate ssDNA probe-surface adsorptive interference. In these cases, sufficient ssDNA surface access is available for probe-surface binding that this interaction hinders subsequent hybridization.[38, 42] ssDNA chain-surface adsorption makes the probe unavailable for target duplex formation, compromising assay performance in a graft density-dependent way. This is reversible in some cases when competing surface-adsorbing and space-filling surface-active diluents are used to displace weak ssDNA-surface physisorption, prompting grafted chain reorientation and improved accessibility to target.[42, 75]

The ssDNA probe brush thus formed on surfaces affects both the hybridization isotherm and the duplex rate conditions, depending on its density, thickness and media. In particular, the brush lowers both the hybridization rate and the attainable hybridization efficiency (yield) for a given concentration of ssDNA targets.[51] Therefore, DNA microarray design should carefully consider probe density influences on target uptake in formulating protocols for array preparation and hybridization as well as in the analysis of assay results. Specifically, surface chemistries are sought for ssDNA probe binding that improve ssDNA surface coupling efficiency and lateral homogeneity, and minimize non-specific binding from

undesired cross-reactive groups intrinsic to many ssDNA combinations with surfaces.[76] Importantly, various surface modifications to improve ssDNA-surface binding have evolved from original affinity reagent printing and desiccation on intrinsically ssDNA-adhesive surface chemistries (i.e., nitrocellulose, glass), thicker, three-dimensional chemically reactive films (i.e., immobilized hydrogels, sol-gels) coated over solid glass supports, and array-patterned photochemical and electrochemical immobilization methods.[25] Detailed descriptions for strategies for microarray and design fabrication, as well as array detection methods, are available.[24, 77]

5. Microarray assay signal detection

Despite the diversity and mature development of ssDNA array immobilization methods and substrate chemistries, the conventional detection method for screening duplexed array signals has remained primarily the conventional fluorescent scanner. This signal typically derives from dye-labeled ssDNA targets derived from PCR-amplified samples prepared with dye-labeled nucleotides that produce surface-bound fluorescent signals complementary to probes placed in different spatial locations. Importantly, integrated fluorescent intensity within each spot becomes the assay “answer”, ostensibly reflecting gene presence and abundance in such assays. Nonetheless, microarray fluorescence data generally do not reliably quantify each gene’s absolute abundance. This is attributed to the effects of different hybridization rates and efficiencies for different target strand sequences and base contents, as well as both variable steric and electrostatic influences of densely printed probes at surfaces. Assay fluorescent signal from a given array microspot is generally arbitrarily judged to be significantly different from baseline (i.e., normal expression) if different than two log orders in spot intensity (increase or decrease in relative fluorescent units, S, i.e., 2log *S*).[78] Assay detection limits and relative noise levels vary, depending on substrate, probe length, target length, detection milieu and spotting method. Routine conventional fluorescence scanner images provide information for integrated spot pixel intensity, shape and morphology, but lack important details for incorporating intra-spot ssDNA immobilized heterogeneity and intra-spot structural issues known to affect both target capture signals and duplex hybridization kinetics critical to this assay’s answer development and diagnostic reliability.[34] Additionally, signal quantitation is affected by numerous, known surface issues and background noise sources that confound reliable, quantitative correlations of spot-to-spot fluorescent assay signals and experiment-to-experiment comparisons.[17, 79] Significantly, integration of spot fluorescent intensity to report assay signal with commonly used fluorescence scanners demonstrates that the typical fluorescence scanner cannot discern microspot optical heterogeneity and fluorescence intensity variations within single printed spots to yield a reliable metric.[80] High resolution chemical state imaging surface mass spectrometry (TOF-SIMS) studies of printed ssDNA microspots confirm that fluorescence scanning analysis fails to reliably report absolute quantitation of immobilized ssDNA probe amounts. Inaccuracy in this fluorescent metric is attributed to fluorescent dye-dye and dye-surface interactions, leading to quenching of surface fluorescence signal.[34]

6. DNA chain states on surfaces as a key feature for performance

Many factors affect DNA microarray performance quality (Table 1) aside from the stringency that affects analytical figures of merit (i.e., sensitivity, specificity) through probe design, sequence selection, and target affinity (shown in Figures 2 and 3). A major influence comes from ssDNA immobilized chain “states” that directly affect probe “availability” to target binding at surfaces. Hybridization processes and DNA duplex formation (i.e., duplex kinetics, thermodynamics, and efficiency) are directly affected by ssDNA chain physical states on surfaces. Factors such as ssDNA length, sequence, grafted probe density, electrostatic interactions, segment conformational states and steric hindrance are critically important to assay signal generation.[34, 80, 81] These intrinsic properties of ssDNA chains at surfaces are reflected in physical manifestations of ssDNA chain persistence length and radius of gyration. ssDNA conformations both hydrated and dessicated on surfaces, in solutions with various ionic strengths, with printed surfactants in print buffers and with dye labels further dictate the biophysical properties of tethered ssDNA on surfaces and resulting interactions with targets. Additionally, target fluorescent labels necessary for fluorescent DNA assay can produce dye-dye, dye-surface, and dye-DNA aggregation non-idealities that also influence fluorescent signal generation.[82, 83]

A last consideration in this regard is that non-equilibrium drying of printed DNA solution spots during ssDNA droplet-based immobilization (Figure 4D) often leads to coffee ring and Marangoni convection flow drying effects that alter dried ssDNA immobilized density and distributions within final probe spots.[33, 84] As probe lateral distribution affects target capture to these spots, kinetically, spatially, and spot-to-spot, these spot-drying artifacts represent a source of DNA assay variability within spots and spot-to-spot with a fundamental and well-studied history.[85, 86]

In summary, inherent variables in the chemistry and physics of ssDNA immobilization and its resulting properties at surfaces are correlated to currently observed limitations in the information content and reliability of DNA microarray assays. Understanding of and control over ssDNA-surface interactions are therefore key for improving microarray assay reliability, quantitative capability and detection limits as well as for developing new microarray surfaces more effective in performing in complex media. Nonetheless, careful analysis linking known bulk ssDNA biophysical properties to ssDNA-surface behavior is rarely reported. This review seeks to describe the current knowledge base in this theme to help identify the fundamental issues affecting DNA-DNA recognition and binding at surfaces. Such knowledge will move more of these technologies to diagnostic applications. A further benefit is a more general extension of this critical review process and analytical rationale to emerging, analogous opportunities in saccharide, cell-based, high-throughput drug screening arrays, and protein-based capture assays.

7. DNA biophysics – a primer

Because ssDNA oligomer probes are densely immobilized at surfaces in microarray formats, their chain-chain interactions, chain-surface interactions, hydration, response to changing ionic strength, drying and other hybridization conditions all impose forces that alter ssDNA

chain conformations and segmental densities at surfaces differently from ssDNA chains in bulk solution.

7.1 ssDNA chain structure and conformational forms

ssDNA oligomers of 20–70 nucleotides are routinely used in arrays and bead-based assays.[26] Immobilized ssDNA probes up to 200 bases long can be purchased commercially (Agilent). As surface-tethered systems, immobilized ssDNA chains will assume an array-dependent equilibrium conformational state at surfaces responding to their immobilization state and local thermodynamic stimuli. ssDNA chains are either described as highly negatively charged, long, semi-flexible or short, rigid polymers based on their length. As a polyphosphate with regular anionic group repeats bridging each nucleotide monomer, they have some properties characteristic of a typical polyanion with fractional, incomplete charging. While longer ssDNA chains can be considered to be semi-flexible polyelectrolytes, shorter ssDNA chains are charged, rigid rod-like structures. For ssDNA lengths > 150 bases, the ssDNA chain is generally recognized to exist as a flexible polymer and for lengths < 150 bases, it is considered as rod-like (based on the persistence length for DNA in physiological conditions: L_P= 50nm or ~150 bases). As a strongly charged polyelectrolyte, DNA's electrostatic interactions are screened by counterion condensation.[87–89] The charge dependence of DNA persistence length and the role of electrostatics in mediating ssDNA stiffness can be altered by varying surface chemistries and components in assay buffers.

The worm-like chain (WLC) model is often used to describe the intermediate behavior between a rigid rod and a random coil to account for the striking local stiffness but long-range flexibility of ssDNA.[90, 91] The WLC model describes ssDNA molecules at low applied forces as an entropic spring and an inextensible worm-like chain, and at higher applied forces (i.e., 6pN to ~70pN) as behaving like an elastic rod.[92, 93] Development of this model for ssDNA and other semi-flexible (or semi-stiff) polymer chains has been an important contribution of polymer theory. It can be modified in various forms to account for other theoretical and experimental variables. ssDNA's flexible chains form diffuse adsorbed layers extending from the surface into bulk solution in contrast to typical semi-flexible or rigid chains forming dense and compact surface-adsorbed layers. ssDNA chain coiling (chain flexibility based on the Kuhn length, i.e., 2 times the chain persistence length), conformational degrees of freedom based on solvent conditions (Flory theory of polymer-solvent interactions, excluded volume effects), repulsive interactions between ssDNA electrostatic components, and the chain spring constant reflecting the chain elasticity all describe the ssDNA chain conformation states when tethered at the liquid-solid interface.

7.2 Parameters used to describe DNA physical properities

Physical properties of ssDNA and dsDNA are primarily a function of their chain lengths and solution conditions. Flexibility of both ssDNA and dsDNA chains depends on chain persistence length (L_p), radius of gyration (R_g), and chain flexibility angle (θ), as shown in Figure 5. Persistence length provides a measure of the rigidity of a linear polymer and is evaluated by determining how quickly the orientation of a polymer backbone changes as its chain contour is traversed. Shorter persistence lengths reflect greater chain conformational

freedom. Polymer radius of gyration (R_g) is a measure of the volume occupied by the linear polymer under equilibrium conformational conditions and is evaluated by calculating the time average of the root-mean-square distance of the polymer components from its centroid. The chain flexibility angle (θ) is a fixed bond angle constraining the rotational flexibility around the chain backbone, resulting in chain stiffness. As the bond angle is reduced, the persistence length increases dramatically. Figure 5 schematically correlates chain contour length (L) and persistence length (L_p), radius of gyration (R_g) and the angle of flexibility (θ) for ssDNA and dsDNA tethered to a substrate. The relationship between R_g for ssDNA considered as a semi-flexible chain and persistence length L_p is given by: where L_p/b is the number of monomers in a persistent segment.[37]

$$R_g \approx \left(\frac{N_b}{L_p}\right)^{3/5} L_p \quad (4)$$

The Flory scaling exponent for a solvent-swollen chain with excluded volume interactions (3/5) in good solvent is retained. Chain persistence length for ssDNA (10≤N≤70 nucleotides) ranges from 1.5 nm in 2 M NaCl to 3 nm in 25 mM NaCl, demonstrating the effect of charge screening on ssDNA chain flexibility.[94]

7.3 ssDNA persistence length

Persistence length is used to characterize the flexibility of linear macromolecules and their conformations in the absence of excluded volume interactions. The persistence length can be considered as the length scale above which chains behave ideally (*vida supra*) but below which they are rigid. Persistence length provides an estimate for the typical curvature radius of the polymer chain under thermal fluctuations.[95] Various models (i.e., WLC, Monte Carlo simulations) and experimental methods have been used to report persistence length for ssDNA and dsDNA. The WLC model characterizes the bending length scale of a semi-flexible polymer as persistence length, (L_p), mathematically defined by the decay length of tangent-tangent angular orientational correlations along the chain. The energy required to bend a semi-flexible polymer over an angle (θ) over length (L) depends on chain chemistry, the temperature and persistence length, L_p, of the polymer.[96] The rod's local direction de-correlates at distance(s) along the curve according to e^{-s/L_p}. For contour lengths $L \geq L_p$, ssDNA can be described as a flexible polymer (essentially a self-avoiding freely jointed chain) whose entropic component of free energy is dominant. In contrast, for contour lengths $L \leq L_p$, ssDNA is asserted to be more rod-like, with an elastic-dominated energy (see Figure 5); the stiffer the chain, the longer the persistence length.

Both dsDNA and ssDNA bending rigidities are also described by the WLC model for a polyelectrolyte.[97] dsDNA shows a reduced persistence length when DNA-binding proteins reduce the normal DNA bond angle of 120° to 114±21° in 50mM Na^+ ion salt solution.[98] The dsDNA contour length increases from 0.34 to 0.397 nm/base, independent of salt concentration.[99] The electrostatic influence on persistence length originally expressed in Odijk-Skolnick-Fixman (OSF) theory is the sum of bare persistence length (L_{Pi}) resulting from the intrinsic chain rigidity, and an electrostatic contribution (L_{Pe})

depending on media ionic strength (where $L_P=L_{Pi}+L_{Pe}$).[100] Electrostatic persistence length (L_{Pe}) for polyelectrolytes like DNA is proportional to the Debye screening length (κ^{-1}) and inversely proportional to the Bjerrum length (l_B) (0.7 nm in water/monovalent ions) as $L_{Pe} = \kappa^{-1}/4l_B$. OSF theory estimates for the energy required to bend a straight charged chain show that screened Coulombic interactions led to very high induced chain stiffness.[101]

Single molecule experiments such as optical[93] and laser[102] tweezers in various buffer conditions have been used to study DNA rigidity. In monovalent salt (e.g., $Na^+_{(aq)}$), the measured ssDNA persistence length is consistent with an electrostatic contribution that varies inversely with the ionic strength.[103, 104] The persistence length for ssDNA (e.g., oligo-dT in the range between 10 and 70 nucleotides) decreases from 3 nm at low salt (25mM NaCl) to 1.5 nm at high salt (2M NaCl).[94] Using FRET and SAXS measurement of ssDNA, Chen et al.[105] showed that Mg^{2+} cation is approximately 20–40 times more efficient at charge screening than Na^+ ion in terms of ionic strength (60–120 times in terms of cation concentration). The persistence length of ssDNA (dT40) in NaCl (monovalent 0.1M) is ~ 1.6nm and for $MgCl_2$ (divalent, 0.1M) is ~0.9nm. In a range of moderate-to-high ionic concentrations (~0.1 to 1M salt) dsDNA persistence length drops noticeably by ~25%. [106] Persistence length shortens with increasing ionic strength due to the complex interplay of both chain conformation and ionic strength. OSF theory fails with multivalent cations like $Co(NH_3)_6^{3+}{}_{(aq)}$ and $spermidine^{3+}{}_{(aq)}$. Measurements with these ions gave apparent L_{Pe} values some 25–30 nm lower than the $L_{p(i)}$ (intrinsic) persistence length, as the dsDNA locally bends towards the transiently bound multivalent ions, shortening the intrinsic persistence length[102].

7.4 Radius of gyration (R_g) and ssDNA conformation

Free ssDNA in aqueous solution is generally considered a relatively well-behaved polymer based on conventional polymer physics models.[93] Early experiments deducing ssDNA's radius of gyration (R_g) in buffered aqueous solutions showed R_g to be a function of weight-average molecular weight (M_w),[107] consistent with both Flory and blob models (*vida infra*). This relationship between R_g and M_w was derived from experimental data and Monte Carlo simulations incorporating the Kratky-Porod persistence chain model, and is schematically shown in Figure 6A. As one example, ssDNA of 5000 bases in solution has an R_g of 30nm.[108] Long ssDNA under high salt conditions also behaves as a flexible coil-like polymer,[109] however, these values reflect bulk solution properties in dilute DNA solutions where DNA-DNA intermolecular interactions are not involved and where chain-solvent and intra-chain energetics determine chain conformations in isotropic milieu. ssDNA surface immobilization or adsorption relevant to array formats alters the chain R_g due to new interactions with the impenetrable surface and lateral chain-chain surface crowding where chain-chain interactions appreciably affect chain morphologies, brush-mushroom regimes and resulting layer thickness, H (Figures 6B and 6C).

The presence of an impenetrable array substrate profoundly affects immobilized ssDNA chain conformation and segment distribution with N segments attached ideally by one end at a tethered surface density, σ (see Figure 4). Surface forces resulting in enthalpic interactions

dictate this adsorbed-state chain conformation in each case, balancing long-range electrostatic, medium range dipolar and hydration forces, and short-range dispersion and hydrophobic forces between ssDNA and substrate chemistry versus those for ssDNA and solution in more ideal terms. However, this analysis does not consider the unusual history of ssDNA-surface interactions during array fabrication. This arraying treatment often includes ssDNA nanodroplet solution deposition onto a substrate, non-equilibrium spot drying onto the solid substrate under increasing ionic strength, desiccation, subsequent aqueous rinsing in high ionic strength media, and desiccation again, then final exposure to sample where rapid rehydration and hybridization must occur. This atypical wet-dry processing of immobilized ssDNA produces considerable opportunities for unusual, even irreversible, ssDNA-surface interactions and adsorbed states beyond consideration in classical 2-body treatments. When interactions between ssDNA segments and the substrate are repulsive, scaling theory for isolated end-tethered polymers predicts a depletion zone of ssDNA segments near the surface in the absence of ssDNA-surface adsorption enthalpy. This is characterized by chain segment distribution, $\rho(z)$, increasing as $\rho(z) \sim z^{1-\nu/\nu}$ with the distance *z* from the substrate[110] (shown in Figure 6) and ν is the Flory scaling exponent. At larger z distances, the influence of the surface weakens and the chain segment distribution approaches a maximum value $\rho(R_g) \cong \sigma\ (n)R_g$ -- the average segment density within the polymer layer whose height, H, is approximately given by R_g of the free, unperturbed chain, where n is the number of segments attached to it by one of its ends at a tether surface density of σ.[51, 111, 112] Beyond this $z \sim R_g$, the segment distribution falls off normal to the surface. Hence the ssDNA tethered chain for lengths of at least 1000 bases exhibits a maximum chain density at a distance well-away from the surface, not at the surface.[59]

The reduced chain segment distribution close to the substrate, together with its faster decay for distances $z \geq R_g$ suggests that the chain segment distribution of an end-tethered polymer in the low-density limit (i.e., $\sigma R^2_g \leq 1$) is distinct from its bulk solution form (Fig. 6A) and is strongly asymmetric, resembling the shape of a mushroom (compare Fig. 6A with Fig. 4B and Fig. 5B).[113] Lehner et al.[112] measured segment distributions of end-tethered polymers with uniform chain length in a good solvent using confocal fluorescence microscopy on isolated ssDNA labeled with dye to evaluate the chain conformations. The segment distribution $\rho(z)$ as a function of distance from the substrate, z, measured for chains with contour lengths of $15.4\mu m \leq L \leq 59.4\mu m$ showed persistence length as $R_g \sim L_p^{0:57\pm0:05}$ supporting the presence of excluded-volume interactions between charged ssDNA segments.

ssDNA chains have been shown to adsorb laterally on surfaces with no chain-chain interpenetration, with R_g estimated as $0.38\ N^{1/2}$nm, where N is the number of ssDNA nucleotide bases.[108] At high ionic strength (0.1M salt), ssDNA probe surface density is proportional to the reciprocal of the effective cross-section of a DNA probe coil, $1/R_g^2$, corresponding to an inverse dependence on its length, N, i.e., probe surface density ~ 1/N. [34, 81, 108] Longer ssDNA probes exhibit flexible coil behavior (i.e., $R_g \sim N^{1/2}$) in high ionic strength solution (measured for ssDNA 280 to 5380 nucleotides long where the Debye length is sub-nanometer.[108] This provides two insights; 1) that ssDNA dimensions on surfaces are different than that of their respective bulk states at high ionic strengths, and 2)

this distinct difference in bulk (i.e., target) versus surface (i.e., probe) ssDNA chain dimensionality affects their ability to hybridize.[114, 115] Another profound outcome is that ssDNA surface coverage decreases with N over the entire ssDNA size range investigated, dropping by nearly an order of magnitude from ~6 $\times 10^{12}$ probes/cm^2 for 8-mer ssDNA probes to ~7$\times 10^{11}$ probes/cm^2 for 48-mers.[81] At low ionic strength, temperature-dependent stiffening of ssDNA is rationalized by combining counterion condensation theory with the OSF description of the electrostatic persistence length and the unstacking of bases at elevated temperatures.[116] [87] Steel et al.[81] showed that surface coverage of DNA probe strands longer than 24 bases begins to decrease notably with increased probe length, consistent with less ordered surface arrangement of DNA chains, reflecting increasingly polymeric behavior.

7.5 Electrostatic effects on ssDNA chain properties

Manning's counterion condensation concept for highly charged polyelectrolytes, including ssDNA, essentially condenses counterions near charged polymer surfaces.[88] The approach was proposed for rod-like polyions with large persistence lengths as a conceptual framework, not as a predictive theory. The condensed counterion layer is sufficient to neutralize ~76% of DNA formal charge, reducing the anionic charge of each phosphate to −0.24e; divalent and trivalent counterions reduce residual phosphate charges to −0.12e and −0.08e, respectively[88] but these cations also induce altered DNA bending states (*vida supra*). In doing so, the electrostatic contribution to DNA stiffness is reduced by phosphate backbone charge screening under counterion condensation.[71, 87] Cation binding to DNA is an ion-exchange reaction, releasing other counterions into bulk solvent and providing favorable entropic sources of binding energy. Schurr et al. [89] complemented this theory using experimental data comparisons with theoretical models with polyelectrolytes, showing the effects of counterion condensation on ssDNA configuration at surfaces. Other experiments show that supercoiled dsDNAs in solution deform farther from their minimum energy configuration than corresponding surface-confined dsDNAs, with the number of configurations available in solution dsDNA vastly greater than surface-confined DNA.[89, 117, 118] Optical tweezers experiments showed decreasing dsDNA persistence length for increasing counterion valence[102] meaning that dsDNA is more flexible with increased counter-cation valency. Manning also proposed contributions of DNA's phosphate anion charge to DNA stiffness; dsDNA helical configuration represents an equilibrium between stretching forces caused by inter-phosphate repulsion and compressive forces caused by attractive interactions between Hoogsten or Watson-Crick base-paired nucleotides.[119] Thus, the strong dependence of both ss- and ds-DNAs' persistence lengths on salt concentration and resulting chain condensation is manifest through double layer screening interactions. Recent observation of major conformational changes for a ssDNA brush (968 bases) confirmed the universal scaling of polyelectrolyte brush height as a power of 1/3 with density-to-salt ratio. However, the actual effects of DNA charge on the molecular rigidity of DNA are debated.[120] Theoretical and experimental results have shown that DNA conformation depends on the local molecular-level charge balance.[121] X-ray crystallography experiments involving tethering of cations in the major groove of dsDNA (directed radially outward) suggested that these cations mediate chain bending and dsDNA collapse through electrostatics without disrupting base stacking.[19] Thus, both phosphate

neutralization and adduction (cations bound to major grove) induce spontaneous dsDNA bending,[121, 122] with influences on persistence length and layer thickness as described (*vida infra*).

Dramatic reductions often observed in immobilized ssDNA hybridization efficiency and thermal denaturation curve broadening as immobilized probe surface density increases are attributed to the so-called Coulomb blockage.[123] Intra-chain Coulombic repulsion between like-charged ssDNA nucleotides in immobilized probes in crowded surface packing results in a more extended and swollen chain conformation. Inter-chain charge-charge repulsion is a natural consequence of laterally immoblized ssDNA, adding to steric forces in compelling immobilized ssDNA to stretch away from the surface, subject to local chain rigidity and conformational limitations. High local field strengths are expected from these high charge densities fixed on surfaces via DNA arraying. On metal surfaces (e.g., thiolated ssDNA on gold) this also generates image charges.[121] This considerable negative electrostatic barrier leads to surface repulsion of incoming ssDNA target as well. These local opposing surface potentials must be mitigated to enable duplex formation with incoming targets of like charge density, and also limit lateral probe-probe interactions that would interfere with hybridization. This necessitates use of high ionic strength printing and hybridization buffers and wash solutions to screen charge density and enable shorter-range duplex hydrogen bonding through short ssDNA oligomer base complementarity. Additionally, steric barriers to duplex formation are introduced by the short, rigid, dense ssDNA chain densities arrayed on surfaces. Electrostatic contributions to ssDNA stiffness are reduced by phosphate screening (i.e., counterion condensation).[71, 124] Local ssDNA deformability (softness) with respect to chain bending due to excess cation-ssDNA binding[121] both help induce spontaneous DNA bending and twisting to alter chain conformations in a ssDNA sequence-dependent manner.[125, 126] These are proposed to facilitate statistical sampling of multiple chain states between surface and bulk ssDNA pairs to produce duplexes. Probe ssDNA-surface interactions that produce multiple ssDNA surface-adsorbed states (i.e., loops, trains, and tails)[127] or induction of ssDNA secondary structures confound this ideal duplexing situation: entire probe strand sequences may not be available to bind target if adsorbed to surfaces or too stiff to accommodate incoming target encounters required for duplexes.[80] Control of probe conformation and orientation is therefore essential to ensure high pairwise reactivity, orientation, accessibility, and stability of the surface-confined probe, and to avoid nonspecific binding.[25] Conformation and orientation of ssDNA probes on gold surfaces have been extensively studied by varying ionic strength, temperature,[116] length of probes and their linkers/spacers, and monitoring of these probes with magnetic and fluorescent labels[128] indicating that all these factors play a major role in duplex formation.

Substantial differences in hybridization thermodynamics and hybridization efficiency have been reported for ssDNA free in solution versus surface-tethered DNA (i.e., for both glass and gold surfaces) due to transport, steric (i.e., probe density) and predominant electrostatics effects.[80, 111] Comparison of data obtained from commercial microarrays suggests that solid-phase hybridization is less thermodynamically favored than hybridization of the same sequences in solution.[129] At lower ionic strengths, an electrostatic balance between the

concentration of immobilized oligonucleotide charge and solution ionic strength governs the onset of hybridization. The electrostatic repulsion of the target nucleic acids from the probe array dominates the binding thermodynamics, causing the Coulomb blockage of the hybridization leading to dramatically decrease both hybridization efficiency and thermal denaturation curve broadening as probe surface density increases.[123] With increasing ionic strength, the electrostatic dominance diminishes and hybridization behavior becomes more complex.[73] Suppression of hybridization affinity constants relative to solution values, and their weakened dependence on the concentration of DNA counterions have indicated that the immobilized strands form complexes that compete with hybridization with analyte target strands.

For a typical hybridization assay on ssDNA-immobilized glass surfaces under conditions near pH 7 in salt content of 1 and 0.1M, the surface potential is −35 and −80 mV, respectively.[130] At a high probe density of 3×10^{13} per cm^2 in an ionic concentration of 0.3M salt, the maximum electrostatic potential in the ssDNA probe layer is ~130 mV.[131] This repulsion increases further as DNA duplexes are formed with the probe layer (i.e., charge density increases), accompanied by crowding and steric issues, and suppresses further hybridization with Columbic blockage and reduced microarray efficiency and sensitivity.[123] Hence, Coulombic screening using high ionic strength hybridization buffers and multivalent counterion enhancement can mitigate some of these adverse effects by reducing Debye lengths.[132] Nonetheless, their effects on DNA probe and target molecular conformations are frequently not considered in influencing how probe and target must interact to duplex.[133] Use of three-dimensional arrays using probe immobilization in gels, mimicking aspects of solution hybridization, can also reduce these effects on DNA duplex formation.[134] Alternatively, reduced DNA chain-chain repulsion and enhanced hybridization kinetics at surfaces have been achieved by applying a positive electrostatic potential to ssDNA-immobilized surfaces, leading to claims for increasing assay sensitivity and stringency by reversing the field once hybridization is achieved to repel all mis-matched pairs with reduced binding affinities.[135, 136]

Schematics showing Coulombic blockage by ssDNA on surfaces and the dependence of R_g on ionic strength (ion valence of Z) are shown in Figure 7. Two different scenarios emerge in the charged brush regime characterized by two length scales: the average vertical ssDNA extension from the surface, H, and the typical extent of the counterion cloud thickness, denoted by x shown in Figure 7. Counterions can either extend outside the brush, x > H, as shown, or be confined inside the brush, x H. In the weak-charge limit, the counterion cloud has a thickness x larger than the thickness of the brush layer, H. For the strong-charge limit, where all counterions are contained inside the layer, the brush and cloud have a single length scale, x H.[137] As shown in Figure 7 (left), ions pass freely between the layers and the external electrolyte for case (x > H). The ssDNA chains provide a constant negative charge density inside the brush, producing a local electric field interacting with salt ions referred to as the proximal region. In a brush regime, the surface field decays and is zero. The Debye length (electrostatic screening) with the ssDNA layer is sufficiently less than the layer thickness, H. Neutron reflectivity measurement indicated that for 25mer oligonucleotides at coverage of 3×10^{12} cm^{-2} in 1M NaCl, the Debye length (κ^1) is below 0.2nm.[132] The influence of ionic strength on the flexible chain of R_g is depicted in Figure 7. The ionic

strength (Z) and R_g have inverse relations due to chain condensation with added salt, affecting the probe and target chain conformations, and probe R_g influencing duplex formation. Different buffer salts influence probe immobilization efficiencies and kinetics. Petrovykh et al.[138] showed that buffers with divalent salts dramatically increase the efficiency of immobilization and result in high immobilized surface densities.

7.6 ssDNA Bending and Elasticity

ssDNA chain stiffness opposes interaction processes in duplex formation requiring bending, twisting, and looping typical for conformationally induced hybridization.[139, 140] As both ssDNA probe accessibility and target binding affinity are key parameters affecting hybridization efficiency in surface-based biosensor technologies, improved chain accessibility and flexibility result in higher hybridization efficiency.[141] The classic framework for understanding long-range ssDNA shape and resistance to bending is explained fairly well by the WLC for ssDNA flexibility.[19] Marko and Sigga [142] described the free energy required to deform a stiff helical, symmetrical DNA molecule to explain the bending and twisting of ssDNA with elastic theory. Cluzel et al.[143] measured ssDNA bending by the movement of the micropipette tip causing the tethered ssDNA molecule to be stretched between the optical fiber of known stiffness and the bead with the applied force proportional to the measured bending for a known stiffness of the optical fiber. Willam and Maher [121] explained DNA bending using electrostatic theory for chain phosphate neutralization and excess cation binding to the major grove of DNA, inducing spontaneous molecular bending. Local ssDNA bending and chain twisting is also sequence-dependent.[125, 126] Both kinked WLC (KWLC) and single-stranded bubble models propose local distortions that could strongly enhance DNA bending and bidirectional molecular torsional flexibility.[144] ssDNA solution conformation is often described using statistical approaches such as flexibly jointed or WLC models.[94] However, dsDNA distortion such as formation of circles smaller than ~85bp which include sharp dsDNA bending or kinking cannot be explained with the WLC model.[145, 146] Thus, while models and simulations for both ss and ds DNA chain dynamics and conformations can be used to explain certain experimental data, they are often limited in accuracy, case-specific and not universal. This is particularly true for short ssDNA tethered chains at surfaces. Similarly, the forces (or, more likely, balance of forces) responsible for ssDNA's unique bending stiffness remains unresolved,[19] also for immobilized strands at surfaces. The fundamental forces responsible for the remarkable resistance of DNA to bending and twisting remains controversial.[19]

Zhang et al. [147] studied ssDNA elasticity through Monte Carlo-based implementation of a modified freely jointed chain (FJC) model with electrostatic, base-pairing, and base-pair stacking interactions. In low-salt solution, electrostatic interactions dominate while at low forces, the molecule can be more easily aligned than an unmodified FJC. In high-salt solution, secondary hairpin structures appear in ssDNA by self-complementarily while external stretching induces a hairpin-coil structural transition that is continuous for ssDNA made of random sequences. Their modeling calculations along with experimental data indicated that base pairing of ssDNA tends to form a nested, independent planar hairpin structure rather than a coiled in solution. These results demonstrate that increased ssDNA

accessibility increased dsDNA hybridization efficiency using pH- and salt- driven bending of ssDNA probes.

7.7 Factors influencing DNA persistence length

Chain persistence length varies depending on whether chains are bound to surfaces or in bulk solution, with various surface interactions, temperature, type of buffer, divalent or multivalent ions present, and also based on the method of measurement.[148] For example, the apparent persistence length (L_{pa}) of dsDNA assessed using AFM is much shorter on 3-aminopropylsilane layers over mica (zeta potential > 0 mV) than on bare mica (zeta potential < 0 mV). The same surface effect has also been shown qualitatively for plasmid DNA with L_{pa} of dsDNA varying from 55 to 100 nm on bare mica and from 20 to 40 nm on AP-mica surfaces.[149] Persistence lengths measured by different methods vary considerably: the dsDNA L_{pa} value measured by electron microscopy is 150 nm in 30mM ammonium acetate[150] in minimum salt concentration, whereas it is 35–50 nm in solutions with Mg^{2+} cation concentrations above 0.1mM.[151] Additionally, the experimental persistence length does not correlate well with simulations (consistently less than experimental values) since the persistence length is highly sensitive to factors such as base sequence, hairpin loops, and differences in experimental methods (typically fluorescence spectroscopy, laser tweezers, and gel electrophoresis). Under physiological conditions, conventional ssDNA values for L_p are near 50 nm or ~150 bases. Evidence also suggests that sequence-dependent differences in base stacking forces can measurably influence ssDNA persistence length. However, the scale of these stacking effects has never been experimentally compared with electrostatic effects.[152, 153]

7.8 Persistence length of ssDNA tethered to surfaces

Understanding the structure of ssDNA tethered to surfaces is critical for optimizing its accessibility and binding to target ssDNA, influencing hybridization rates and efficiencies, and ultimately assay signal quality and reliability. While a substantial literature exists on ssDNA L_{pa} in solution, relatively few measurements of ssDNA persistence lengths tethered to surfaces are reported, despite the implications of chain conformational dynamics, mobilities and mechanics on duplex formation. Calculations of ssDNA persistence length based on a coarse-grained model is dependent on chain length.[154] For a small, identical number of bases, ssDNA has a longer end-to-end distance (0.64 nm distance between bases) compared to dsDNA (i.e., 0.34 nm inter-base distance for coiled base-paired duplexes). However, adding more bases, ssDNA yields shorter end-to-end distances than dsDNA because it curls over on itself much more on average, reflecting its shorter persistence length (≈1.48 nm).[155] Some experimental and simulation approaches have evaluated DNA persistence length as a function of temperature, salt concentration, base sequence, interaction potential strength, and local position along the chain. ssDNA persistence length tethered to a modified graphite surface using atomic force microscopy at very low ionic strength was L_p = 9.1 nm and this decreases with increasing ionic strength to 6.7 nm and 4.6nm at 1mM and 10mM NaCl, respectively.[108, 156] Murphy et al.[94] used FRET to deduce persistence lengths for ssDNA (oligodeoxythymidylates, dT_N) of chain lengths ($10 \leq N \leq 70$ nucleotides) over a wide range of salt concentrations. Persistence length varied from 1.5nm in 2M NaCl to 3nm in 25mM NaCl. The ssDNA in this case was not bound to a

surface directly but attached to dsDNA immobilized on a streptavidin-coated quartz surface. Chen et al. [105] measured persistence length of dT_{40} tethered to a glass surface at the same ionic strengths as Murphy et al. They however used x-ray and fluorescence methods and found that persistence lengths were 50% less for tethered ssDNA, possibly due to glass surface interaction influences on immobilized chain conformations. Crozier et al.[157] reported the persistence length of ssDNA with molecular dynamics (MD) simulations using a coarse-grained model for single polyelectrolyte chains grafted to a solid surface. This study revealed a small intrinsic persistence length that is highly extended in zero salt simulations. Added salt does shrink the chain as salt ions enter the volume near the chain. Persistence lengths predicted for ssDNA using the coarse-grained DNA model (with bases modeled as rigid-body ellipsoids to capture their anisotropic stereochemistry) initially decreases with increasing temperature in accord with the WLC model; however, at higher temperatures where nonlocal interactions become important, the persistence length shows an increasing trend over a broad range of temperature. Below the crossover temperature (i.e., the transition between expanded and collapsed chain globules), base stacking interactions stiffen the ssDNA chains and increase its persistence length, while above this temperature, nonlocal base-base van der Waals interactions soften the chain and decrease the persistence length.[154]

The persistence length for a homogeneous ssDNA comprising homo-adenine as long as ~50 bases is more than the corresponding homogenous strand of thymine bases ($L_P \approx 2$ bases) at low temperature due to the large enthalpic costs for hairpin formation in poly(A) over poly(T) nucleotides.[125] However, at higher temperatures due to non-local interactions between bases, poly(A) forms a collapsed globule with shorter persistence length while poly(T) forms an expanded globule.[154] Temperature has a drastic influence on persistence length and R_g for both ss-poly(A) and ss-poly(T). Thus ssDNA persistence length tethered to surfaces varies considerably with many factors (temperature, ionic strength, sequence and type of surface immobilization), influencing accessibility and properties for further binding target DNA and important for considering probe accessibility and mobility in the microarray chip design.

7.8 Persistence length of dsDNA at surfaces

Hybridization of ssDNA to form dsDNA is a necessary event required of two complementary DNA strands (probe and target) in a microarray assay. The physical properties of each DNA partner change upon hybridization: dsDNA is much more rigid than its ssDNA precursors.[158] This difference in chain rigidity can be described in terms of altered persistence length.[159] Persistence length of dsDNA has been shown to be ~50 nm in environments containing salt concentrations greater than 10 mM, while that of ssDNA has been shown to be only about 1 nm.[151] As discussed (*vida supra*), ssDNA molecules of lengths less than 50 nm have very different chain rigidities compared to dsDNA molecules of the same lengths, and each as distinct persistence lengths in solutions versus bound states. This several disparate properties must converge in their hybridization at a surface. Stretching persistence length of dsDNA has also been measured using single-molecule techniques.[97, 160] Abels et al. measured individual dsDNA molecules attached at one end to a glass cover slip and at the other end to a magnetic bead, yielding values of 54 nm, in agreement with

other values reported.[95, 97, 161] Brinkers et al.[96] measured persistence length for a lone dsDNA using dark field microscopy by capturing the projected positions of attached nanoparticles undergoing constrained Brownian motion. With Monte Carlo simulation and experimental evidence, the authors evaluated persistence lengths of 45 single molecules of four different lengths of dsDNA measured under high salt concentrations. These had a mean value of 35 nm (standard error of ±2.8 nm). In contrast, Mastroianni et al. measured short dsDNA persistence lengths in solutions with dsDNA-linked dimers of gold nanoparticles using small-angle x-ray scattering without requiring any external forces or binding to a substrate. These results for dsDNA comprising 42–94 bases were consistent with a simple WLC model of dsDNA elasticity and comparable to results from Monte Carlo simulations. A persistence length of 50 nm (~150 bases) is consistent with results from single-molecule force-extension experiments on much longer dsDNA chains. These results contrasted recent suggestions of enhanced DNA flexibility at these length scales.[162] dsDNA persistence length also depends on media ionic strength, similar to ssDNA.

The persistence lengths of both ssDNA and dsDNA have the same functional dependence on ionic concentration. Notably, dsDNA is roughly 55 times stiffer at 0.02M, 25 times stiffer at 0.04M and 52 times stiffer at 0.13M than ssDNA.[108] Extra stability is provided by hybridization since weakening base-base interactions with increasing ionic strength only modestly reduces chain stiffness due to stacking.[154] Decreased DNA persistence length was also observed for increasing counterion valency.[9]

7.9 ssDNA chain elasticity

DNA chain mechanical properties include force extension (stretching), elasticity, torque as a function of twist for stretched ssDNA and torsional strain.[163] ssDNA chain flexibility and conformational adaptation are important factors for duplex formation. Various theories are proposed to understand ssDNA elasticity. The classic framework for understanding long-range ssDNA chain shape and resistance to bending is embodied in the WLC model of ssDNA flexibility in a Kratky-Porod chain (i.e., simple polymer chain with no torsional stress).[164] The elasticity of longer DNA chains including looping, distance-dependent flexibility[165] and J-factor (ring-closure probability for a given DNA length, an experimentally accessible measure of polymer stiffness) are consistently explained by the WLC model.[166]

AFM and optical tweezers have been used to successfully measure DNA stretching under applied forces.[100] Measuring DNA elasticity by tethering DNA to a surface and applying various loads to determine chain elongation and yield points are also well known.[167] Various experimental methods and instruments with newer technologies have aimed at determining DNA’s molecular elasticity. However, dsDNA elasticity is highly influenced by factors such as the type of surface anchor, a duplexed terminal anchored to the material, type of substrate material (e.g., hydrophilic or hydrophobic) and media ionic strength.[168, 169] Changes in ionic strength predict DNA elasticity based on persistence length and elastic modulus determinations. Lowering ionic strength increases persistence length and reduces DNA elastic stretch modulus.[100]

The finite WLC (FWLC) model modifies the classical WLC model by including finite chain length, chain-end boundary conditions and bead rotational fluctuations (inherent in optical trapping assays where beads are used to apply forces).[170] The FWLC solution provides a significant improvement to the theoretical framework used to analyze single-molecule experiments over a broad range of experimentally accessible DNA lengths, including both short contour length (a few hundred nanometers) and very long (microns in contour length) molecules.[170] The freely jointed chain (FJC) model reliably predicts properties for a polymer chain whose segments are unrestricted in their orientation, corresponding to freely rotating segments of the Kuhn length (i.e., $2L_p$). However, the FJC model is not a good approximation for the elastic behavior of DNA molecules at large extensions (i.e., $H > R_g$). [139] The WLC model is much better for describing the behavior of oligo-DNA particularly at large extensions (i.e., for DNA fragments 105–130 bases in length, $H > R_g$). However, dsDNA cyclization studies have revealed the non-applicability of the WLC model to DNA bending on biologically relevant length scales (~85 bases in length). The WLC model cannot describe the force of extension, solution scattering, and long contour-length cyclization experiments, and therefore alteration of the WLC model is required to include sharp bending or kinking of dsDNA.[171]

The elastic properties of both short and long ssDNA and dsDNA tethered to charged and uncharged supports under aqueous conditions are important in defining probe interfacial properties affecting the kinetics, thermodynamics and binding efficiency of DNA target in microarrays. Electrical manipulation studies by Rant et al. of ssDNA and dsDNA end-tethered to gold surfaces in electrolyte solutions showed dissimilar dynamic behavior attributed to elasticity of the bound DNA (flexibility of ssDNA and rod like stiff behavior of dsDNA).[172] Stiff polymers undergo rotation around their anchoring pivot point on a surface (i.e., a cone of polymer occupancy); flexible polymers, by contrast, are pulled onto the attracting surface, segment by segment, leading to ssDNA loops, trains and tails. These features are important determinants of ssDNA accessibility and the ability of self-assembled probes to bind complementary target sequences.

Studies of DNA mechanical properties indicate that DNA's elasticity is similar to that of synthetic polyamide, nylon.[173] Recently, Eijck et al.[174] used neutron scattering through aligned fibers of dsDNA to gauge the speed of sound waves vibrating along DNA helices, yielding a chain force constant (modulus) of 83 N/m. Using a computer simulation model of DNA's vibrations, the authors explained the large variation in previously reported dsDNA elasticities ranging from 0.3 to 133 N/m. Studies of mechanical properties as early as 1995 by Marko and Siggia analyzing stretching of dsDNA tethered at one end and stretched by a force applied directly to the free end by an electric field or by hydrodynamic flow have been compared with a statistical mechanical treatment of the WLC model. All experiments display a strong stretching regime where end-to-end distance approaches the DNA contour length as $1/(\text{force})^{1/2}$, consistent with WLC elasticity.[142, 175]

Experiments with torsionally constrained single molecules provided the first direct measurements for coupling twists and stretches in dsDNA.[176] A constrained twist of a DNA strand manifests itself as a link, twist or writhe due to DNA's elastic entropy.[176] Experiments using torsionally constrained DNA have permitted determination of coupling

between DNA twist and stretch.[91, 177, 178] Results are consistent with fundamental principles predicted from classical WLC elasticity theory. Single-molecule stretch experiments indicate that dsDNA deviates from the inextensible WLC model up to forces of 10pN. Beyond 65pN, dsDNA suddenly changes its form from B to S, stretching up to 70% beyond its canonical B-form contour length. dsDNA's "S form" is stable in high salt up to forces of approximately 150 pN (for random sequences). Some 300 pN above this force, S-DNA melts into single strands that exhibit the characteristic force/extension behavior of ssDNA.[177] The simplest extensible WLC with twist rigidity is considered a model for DNA under tension. However, dsDNA is chiral; demanding that helix stretching coupled with twisting must lead to a structural transition.[97] [84] Force–extension occurs when single DNA molecules are twisted in either direction and pulled to high force [179] and the phase boundaries correspond to the structural states of DNA in coexistence with adjacent pure phases.[180] Stretching of helical dsDNA twists molecule, perturbing its twist degree of freedom and leading to its supercoiling as it relaxes -- a distinct phenomenon occurring in DNA compared to other polymers.

When dsDNA is stretched beyond its contour length, a highly cooperative overstretching transition is observed, dependent on ionic strength. Wenner et al.[181] performed measurements of DNA elasticity and overstretching transition by stretching single dsDNA molecules as a function of monovalent salt concentration using optical tweezers. DNA persistence length with sodium chloride concentration change from 1000 to 2.57mM increased from 46 to 59 nm, with the elastic stretch modulus remaining constant. However, as this salt concentration was further decreased, the overstretching transition force decreased from 68 to 52 pN, attributed to reduced dsDNA double helix stability. Although Watson-Crick hydrogen bonds break as helical DNA is overstretched, these data indicate that both DNA strands remain close together during the transition. Punkkinen et al.[182] theoretically described the salt-dependent over-stretching transition of DNA by coupling the two-state model and the elasticity theory proposed for monovalent salt effects on elastic modulus during the transition. In dsDNA, the effective chain length per unit charge varies with salt in agreement with both the Manning[71] and Poisson-Boltzmann models for thin polyelectrolyte rods[183], whereas the other model parameters describing structural features exhibit little salt dependence.[71] Thus, electrostatic components of force-induced DNA overstretching might be apparently mediated mesoscopically via elasticity[182]. This is an important factor since DNA microarray duplexing assays are conducted typically in high ionic strength buffer and salt systems to minimize electrostatic repulsions while maximizing ssDNA elasticity, extension and accessibility that impact the efficiency of target binding and the stability of resulting dsDNA at surfaces.

DNA solution pH also affects chain extension, efficient hybridization and the stability of the resulting DNA duplex via influences on DNA conformation and duplex stability. Single molecule dsDNA exhibits a highly cooperative overstretching transition under varying pH at high ionic strength.[121] Williams et al.[184] showed that as solution pH was increased from pH 6.0 to 10.6 in 250mM NaCl, overstretching transition forces decreased from 67.0±0.8 pN to 56.2±0.8 pN, while the transition force width remained nearly constant. As the pH was lowered from pH 6.0 to 3.1, the overstretching force decreased from 67.0±0.8 pN to 47.0±1.0pN, but the transition width increased from 3.0±0.6 pN to 16.0±3pN. These

results quantitatively support that DNA strand dissociation, or melting, occurs during the overstretching transition.[184] However, other data suggest that dsDNA should unwind under tension as it is pulled towards its denatured structure.[91, 143, 177, 185] Gore et al. [186] used rotor bead tracking to directly measure twist–stretch coupling in single dsDNA molecules. dsDNA overwinds under tension, reaching a maximum twist at a tension of ~30pN, and when increased above this critical value, the dsDNA begins to unwind. The observed twist–stretch coupling predicts that dsDNA should also lengthen when overwound under constant tension. This property would possibly explain the anomalously large torsional rigidity of dsDNA[186] and might also have implications for surface-tethered DNA since ssDNA must stretch and twist to form dsDNA when duplexing new target to compensate for variability in chain dimensionalities at encounter, and to align bases for optimal hydrogen bonding in duplexes. dsDNA is well-described as a worm-like chain at concentrations of di- and trivalent cations capable of inducing condensation but such condensation is prevented by keeping the dsDNA molecule stretched. A retractile force appears in the presence of multivalent cations at molecular extensions that allows intramolecular contacts, suggesting that condensation in stretched DNA occurs by a “thermal ratchet” mechanism.[102] Using designed sequences of DNA with nearly identical DNA curvatures (based on same length, e.g., 132 bases) with different elasticities and varied AT base pair (i.e., duplex melting point) contents, Raghunath et al.[187] showed that dsDNA persistence length varies by almost 30% between sequences containing 61% AT and 45% AT nucleotides.

DNA, like other biopolymers, differs from classical polymers in its intrinsic torsional stiffness. The force of extension, torque, and angle of DNA for structural and elastic parameters of torsionally melted dsDNA single molecules was measured by Sheinin et al. [188] using an angular optical trap. Under moderate forces, melted DNA assumes a left-handed structure and is highly torsionally compliant. For lower forces, melted DNA properties are highly dependent on DNA sequence.[188] Moroz and Nelson[140] studied DNA force extension as a function of over-twist over a wide range of applied force with a theoretical model. The statistical character of DNA conformations under tension changes from a classical random walk to “torsional random walk” whose random variables are the direction of each step relative to its predecessor, together with a relative axial twist. The similarity between Metropolis Monte Carlo simulation[189] and experimental measurement of torsionally stretched DNA by Strick et al.[91] strongly suggests that correlations observed between base stacking and permanent hydrogen bond constraints play an important role in understanding this supercoiled DNA elasticity. Bryant et al.[163] measured torque as a function of twist for stretched dsDNA: that is, torsional strain in over- or under- wound molecules to power the rotation of sub-micrometer beads serving as calibrated loads. With dsDNA’s twist elasticity, the torsional modulus shows an over- or under-wound dsDNA molecule behaving as a constant-torque wind-up motor capable of repeatedly producing thousands of rotations, and that an overstretched molecule acts as a force–torque converter. These results reflect the importance of external forces on dsDNA. However, dsDNA elasticity and mechanics influences occurring at the microarray surface are not directly comparable to these results since most of these molecular mechanics exercises impose applied forces, extensions and rate-dependent transitional behaviors not relevant to array

duplex formation. Therefore, these effects should be evaluated further for specific effects on target capture, especially the hybridization transitions of ssDNA to dsDNA tethered to surfaces influenced by external factors such as ionic strength and pH.

In summary, absent the application of external extensional forces, short ssDNA maintains a compact conformation consistent with a short polyelectrolyte; its chain extension per base pair is shorter than that of dsDNA for forces smaller than ~6 pN. At higher applied forces, however, the situation is reversed. As the dsDNA single strand is not constrained to follow a helical path in extension, it becomes nearly twice as long as dsDNA as it is pulled in tension, forming brush-like conformations on the surface under applied forces (i.e., shear, tensile, electrical).[97] These chain tensile properties seem to be affected by their surface environment when tethered.[190] However, without external forces, ssDNA chain conformational adaptations in a tethered-state must adapt to accommodate DNA target binding on surfaces by overcoming these local higher chain energies, extending spontaneously from a surface to form an accessible chain capable of rapid target encounter and dsDNA duplex formation that is then much stiffer. dsDNA chains are generally helical with twisted conformations that contain complex torsional and elastic energies exhibiting non-linear chain extension responses to external forces. Rather than extending fully to a brush-like state with forced extension, dsDNA is separated into ssDNA unimers by stretching forces strong enough to cleave chain-chain base-paired hydrogen bonds after torsional and helical elastically stabilized conformational changes are completed.[191]

The longer the DNA chain, the higher the chain polyphosphate negative charge density at assay pH, affecting chain conformational mobility as seen through persistence length and chain mechanical changes that change assay hybridization efficiency.[141] Importantly, longer ssDNA and dsDNA chains respond to ionic strengths and applied electrical forces differently than shorter ssDNA typically used in probe tethering at surfaces (i.e., ssDNA, but also dsDNA).[131] Longer ssDNA chains forms secondary structures that alter strand accessibility and hybridization while shorter chains reduce the sensitivity of detection. Additionally, longer ssDNA probes have Coulombic repulsion and chain-chain steric issues that scale depending on their immobilized density much differently than shorter probes.[51] Since target chain conformations in bulk solution are also distinct from those of ssDNA probes at surfaces, hybridization must change both probe and target chain dimensions and conformations upon encounter, and within the complex double-layer and steric environment of the array surface-immobilized probe, in order to produce a successful assay event. How these molecular properties are discriminated for duplex specificity, or controlled or optimized in current array formats is not understood, at least at the level of fabrication and experimental use.

8. Extending ssDNA and dsDNA tethered chains biophysical behaviors to microarray applications

Determination of tethered ssDNA probe and dsDNA duplex conformations on surfaces and correlated hybridization properties with incoming ssDNA targets provides empirical information required to understand barriers to DNA duplex formation in arrays. This information is difficult to collect but is necessary to rationally move DNA interfacial

applications forward using known surface designs and described behaviors to improve their reliability, and clinical and biotechnological utility in many surface-bound formats. Immobilized ssDNA monolayers are widely used in both fundamental and applied genomics and are also versatile experimental models for elucidating fundamental behaviors of charged polymers at interfaces. The physical behavior of these assay systems is to a large extent governed by internal microenvironments within adsorbed or tethered layers of polyanion ssDNA oligonucleotides, external influences from salts, pH, and temperature, and resulting fundamental intermolecular forces that yield dsDNA duplexes within complex surface states.

ssDNA molecular conformations tethered to a microarray surface significantly affect the rates and efficiencies of hybridization. Many diverse methods have been applied to determine structural features of the immobilized ssDNA layer, such optical or contact methods as ellipsometry[192], optical reflectivity[193], neutron reflectivity[194], x-ray photoelectron spectroscopy[195], FRET[94], SPR[196], and AFM[197]. Many are spatially or time-averaged measurements and intrinsically not very sensitive to variations in ssDNA chain conformations or surface chain densities shown to influence ssDNA molecular behavior (*vida supra*). The ssDNA immobilized adlayer response to alternating repulsive and attractive electric surface fields studied by time-resolved fluorescence measurements of ssDNA and dsDNA end-tethered to gold surfaces in electrolyte solutions shows distinct dynamics for flexible single-stranded oligoDNA probes versus stiff dsDNA. Hydrodynamic simulations rationalize this finding to disclose two different kinetic mechanisms: stiff polymers undergo rotation around the anchoring pivot point while flexible ssDNA polymers are pulled onto the attracting surface segment by segment.[198]

To assess conformations of surface-bound ssDNA, Moiseev et al. used an optical interferometric technique (spectral self-interference fluorescence microscopy) for precise polymer extension measurements.[128] This method estimated the shape of coiled ssDNA, the average tilt of dsDNA of different lengths, and the amount of hybridization by evaluating the average location of a fluorescently labeled nucleotide in a ssDNA layer relative to the surface. The ssDNA conformation varied on surfaces based on differences in ssDNA length, whether dye labeling was at the proximal or distal end of the probe and with the dye labeling position on the ssDNA target.[128] Interestingly, unlabeled 50-bases ssDNA probe strands hybridized with 21-bases ssDNA targets dye-labeled at their distal ends and complementary to either the probe's top or bottom part changed conformations differently. The surface distance of the duplex distal end increased from 5.5 to 6.5 nm for the duplex target complementary to the probe's distal end, different from the proximal duplex conformation relative to the surface.

The local electrostatic environment within a dense, tethered polyanion ssDNA surface layer differs strikingly from ssDNA in solution and affects DNA array behavior (*vida supra*) and that of related surface-focused technologies. Electrochemical techniques have been used to probe the ionic microenvironment within end-attached ssDNA oligonucleotide monolayers (i.e., as ssDNA brushes). Local electrostatic field strengths within these immobilized layers are estimated to be −35 and −80 mV for salt contents of 1 and 0.1M, respectively) for a probe density of 5×10^{12} per cm^2, reflecting the expected substantial local surface potential

from highly phosphorylated nucleotides.[131] Vainrub and Pettitt predicted strong electrostatic destabilization effects for ssDNA immobilized in electric double layers.[136] Retention of counterions by the ssDNA brushes manifests as lowered susceptibility of the interfacial capacitance to external salt conditions. The charging response exhibits signatures of structural reorganization whereby DNA strands stretch or relax with changes in solution ionic strength, consistent with expected physical behavior of charged polymer layers. The quantity of bound ssDNA and strand coverage can be evaluated based on shifts in reduction potentials for redox counterions associated with the ssDNA monolayer.[132] The resulting electrostatic potential for immobilized ssDNA probes is significantly influenced by surface properties. For example, the silica surface charge density in 1M sodium nitrate aqueous solution increases from zero at pH 4 to −0.24 per cm^2 at pH 9.5, corresponding to surface potential ranges from 0 to −100 mV, with the glass/silica surface being prone to static charging.[130] Extensive studies of ssDNA surface potential with change in probe density and hybridization on various surfaces with buffers, pH and sequences have been proven to decrease the electrostatic charging.[73, 199, 200] Further, Shen et al,[132] Fritz et al,[201] and Heaton et al,[202] showed that an externally applied electric field can improve hybridization rates without loss of efficiency, discriminating against mismatched dsDNA duplex formation and also improving electronic control of DNA hybridization and facilitating design of chips avoiding the ssDNA folding problem.

9. Microarray surface-capture assay kinetics

Kinetics of DNA hybridization is well studied in bulk solution, however solid-phase probe-target hybridization kinetics is more complicated.[80] Achieving duplex equilibrium is an important endpoint often assumed for microarray assay analysis. Understanding the actual difference in equilibrium constant ($K_E = k_f/k_r$) between bulk vs. surface hybridization is a key to understanding hybridization kinetics and this assay endpoint. Equilibrium binding constants for solid-phase hybridization differ by many orders of magnitude relative to solution values.[203] Microarray DNA assays use competitive surface reactions between many different immobilized probe sequences with highly varying concentrations of matched and unmatched target strands, influencing the assay equilibrium.[204] Additionally, when the surface density of ssDNA oligonucleotide probes increases, DNA hybridization rates and efficiencies decrease,[51, 203] making true equilibrium endpoints often impractical (i.e., too long) for convenient assay use. Henry et al.[205] reported that rate of forward reaction (k_f) for hybridization of end-tethered 22mers in 0.11M salt was five times slower than in solution when ssDNA probe coverage was 1.4×10^{12} per cm^2, and ten times slower when probe coverage increased to 2.8×10^{12} per cm^2. The free energy penalty associated with inserted charged targets into dense probe layers modifies both the hybridization isotherms and the duplex rate equations: the attainable ssDNA hybridization fractional completion and rate of DNA hybridization are both reduced.[51] Probe design (sequence, length, immobilization chemistry) and hybridization (target designs), the array design and its resulting interfacial characteristics are important parameters for improved performance of the microarray. Hybridization kinetics and equilibrium are influenced by 1) concentration- and sequence-dependent competition between diverse strand-strand interactions, both in target solutions as well as at surface between matched and mismatched duplexes, and 2)

aspects of the array fabrication process (probe printing or deposition and resulting density, conformational states). Possible design parameters include the nature of the surface (i.e., the treatment used to minimize nonspecific adsorption and maximize ssDNA tethering and accessibility), and ssDNA probe design (i.e., length, charge, lack of secondary structure, hydrophobicity and the chemical design/length of spacer chains joining the probe to the surface).

Langmuir isotherm surface treatments for thermodynamic approaches to attaining duplex binding equilibrium and their corresponding duplex kinetic equations for hybridization represent a common starting model for non-interactive probes (i.e., no competing nearest neighbor interactions) when ssDNA probe density is sufficiently low; at higher probe densities, the Langmuir model requires modification.[80] However, this treatment has traditionally been based on ideal DNA-DNA duplex binding analyses and strand-strand affinities based on complementarity of isolated matched pairings in equimolar concentrations compared to that for isolated mis-matched pairings at similar equimolar concentrations, without complications of multi-component strand mixing or competition (so-called strand multiplexing). Real assays have complex competition from targets of different sequences and mis-match affinities in varying concentrations.

Longer targets lead to reduced duplex equilibrium binding constants on surfaces due to incomplete or partial overlap of target strands, incurring an entropic penalty for penetrating the dense probe surface (steric issues), and an enthalpic penalty for polyanion-polyanion electrostatic repulsion.[51] ssDNA probe chain crowding can lead to a brush-like regime, [59](modifying the Langmuir isotherm and kinetics due to free energy penalty associated with brush capture of target compared to less dense, conformationally mobile probe mushroom-type layer densities. Some controversies remain in this regard: while Guo et al. [206] observed that the maximum attainable hybridization fraction increases at higher probe density when the number of bases in the target increases, Su et al. reported slower hybridization as the number of bases in the ssDNA target increases at fixed probe density. [207] Surface diluents and probe spacer/linkers are used to overcome these complications by providing space between or flexibility/mobility within crowded ssDNA chains. For example, surface diluents reactive to gold (e.g,, thiolated surfactants) are mixed into thiolated DNA ssDNA probes, or used to displace ssDNA after gold assembly (e.g., mercaptohexanol,[159] 11-mercapto-1-undecanol,[42] thiol-terminated oligoethylene glycols[42]) to increase the average spacing between probe chains.

Additionally, probe surface area (Σ_0) and the number of bases per ssDNA probe chain become important features in electrostatic field and steric contributions to crowded array spots. Probe densities in typical array spots varies from 1.2×10^{10} (low density) to 4×10^{13} (high density) probes per cm^2, corresponding to molecular probe surface area between 25 $nm^2 \leq \Sigma_0 \leq 830\ nm^2$.[37] With a dsDNA duplex radius of 2nm and a probe lateral spacing, d, of ~0.6 nm, sufficient space should accommodate polyanion reactivity at this density. Labeling of probe and target with signal molecules (e.g., Cy3 or Cy5 dyes, or redox reporters) can also affect hybridization behavior and signal intensity (discussed in detail in a section below). Repeated drying and solution wetting steps in common arraying procedures further complicate immobilized chain interactions with each other within the adlayer and

with the solid support. Hybridization condition variables include the composition of the hybridization solution (ionic strength, salt composition, use of surfactants and pH, all of which practically deviate from conditions used in theoretical DNA brush models, *vida supra*), hybridization temperature and hybridization time (incubation time).[208] Typical hybridization temperatures vary over the range 30–60^{0}C depending on the GC base fractions (i.e., duplex chain melt point). The assay incubation time (i.e., time to hybridization endpoint stabilization) can be very long and variable (i.e., from 2 to 16 hours reported)[30, 209, 210] depending on assay signal sensitivity, duplex bulk composition, target concentration, ionic strength and probe grafting density. Importantly, whether this assay time reflects an equilibrium endpoint or not is critical to the assay answer. The real problem lies in assays of heterogeneous ssDNA targets where diverse sequences, lengths, mixed target and non-target concentrations and possible mismatch duplex co-equilibria confound approaches to a single equilibrium assay endpoint.[203, 211, 212]. Incubation times often vary, different even for similar concentrations of probe and target, but depending on assay conditions and largely influenced by ssDNA probe density distributions and ssDNA sequence and length.[37, 133, 213]

Sensitivity and specificity of hybridization isotherms on ssDNA arrays depend on the important assumption that “perfect match” duplexes form exclusively, and with the same affinity, thermodynamic and kinetic behavior that they exhibit in bulk solution as isolated pairs, and significantly, without any influence from the presence of other ssDNA strands and possible duplexes. However, “real” microarrays operate in “multiplex” mode, where many other ssDNA strands and their possible duplex pairings, even as mismatches with finite metastability, are present and competitively operative.[211, 214] Few studies report deviations for perfect match probabilities or kinetics in the presence of strand multiplex bias where different ssDNA concentrations and relative ranges of strand-strand affinities for a multitude of various duplex reactions compete simultaneously, either in bulk or at surfaces. Several additional essential features of multiplex hybridization must be considered. These considerations are associated with the significant probability of formation of mismatch hybrids (cross-hybridization) brought about by sequence homology with other strands and sequence-dependent stability of mismatch basepairs, especially at non-equilibrium endpoints.[203] Competitive hybridization, both at the surface and in bulk ssDNA solutions containing many sample ssDNA strands, lowers the array sensitivity.[133] Assay noise, represented as non-equilibrium “mis-matched” cross-hybridization from competing ssDNA multiplexed reactions, depends on relative competing strand concentrations, strand sequences and the sensitivity of all mis-matches to temperature, and surface probe conditions. These variables are not controlled in common “real life” arrays (as opposed to lab bench model concoctions), given their multiplex design. Hence, the actual fidelity of capture signals produced from such arrays are questionable unless equilibrium binding conditions and algorithms for predicting confounding multiplexing are implemented.[204]

The DNA-DNA surface hybridization model often assumes a Langmuir form modified for electrostatic interactions within the probe layer. Vainrub and Pettitt’s modeling of molecules immobilized in an electrostatic double layer (at high 1M NaCl and low 0.01M NaCl ionic strengths) for both dielectric and metallic substrates[136] predicted strong electrostatic

effects on duplex kinetics. These studies suggested the feasibility of electrostatic control for DNA hybridization and design of assays to avoid DNA secondary structure folding problems (i.e., self complimentarity). [212] They used linear Poisson–Boltzmann theory for double-layer interactions between an ion-penetrable sphere and a hard plate with variables including binding enthalpy, entropy and equilibrium reaction constants for the immobilized complex. They also developed a mean field model for Coulombic effects in two-dimensional DNA arrays to understand the binding isotherms and thermal denaturation of the double helix.[123] These studies on dsDNA duplex models reveal substantial differences in hybridization thermodynamics between ssDNA in solution and that surface-tethered. Electrostatic repulsion of targets from immobilized ssDNA probes dominates the binding thermodynamics, causing the Coulomb blockage of the hybridization and explaining the observed dramatic reduction in hybridization efficiency and the thermal denaturation curve broadening as probe surface density grows in DNA microarrays.

Chen et al.[215] investigated substrate–ssDNA interaction influences on both thermodynamics and kinetics of DNA hybridization of ssDNA-modified gold nanoparticles (GNPs). They proposed that during hybridization, the target ssDNA in solution does not directly react with the immobilized probe, but rather it is first adsorbed onto the GNP surface, followed by two-dimensional diffusion until it finally hybridizes with an immobilized probe ssDNA. Different duplex melting properties observed between hairpin and random-coil sequence ssDNA strands were proposed to arise from sequence- and structure-influenced interactions between ssDNA and GNPs. Steric hindrance induced by the compact configuration in a DNA hairpin probe prevented interactions with the gold surface, facilitating higher stability of hairpin-formed duplexes on the GNPs.

Deviations or extensions of the Langmuir model for DNA-DNA interactions on surfaces reflect the surface environment encountered by multiple targets at different concentrations multiplexing as cross-hybrid duplexes with different affinities, including mismatches. This leads to widely different approaches to equilibrium for assay endpoints. Predictions of real-time DNA hybridization kinetics in microarrays have been performed by various researchers. Halperin[133] and Bhanot et al.[51] both analyzed effects of competitive surface hybridization for hybridization at a number of spots contacted with multicomponent solutions of targets with no bulk hybridization. Importantly, the result demonstrated that array performance is best when equilibrium is attained. Halperin et al.[37] also analyzed the impact of the brush regime on kinetics of hybridization, indicating that slower kinetics can affect the attained hybridization even after long hybridization periods. Forman et al.[216] analyzed observable selectivity in hybridization and the ability to distinguish perfectly matched and mismatched target sequences that are affected by surface interactions. Hagan and Chakraborty [74] developed a theory describing kinetics of solid-phase hybridization based on polymer theory. Also the effect of bulky fluorescent labels on the hybridization was first considered theoretically by Naef and Magnasco[217] and recognized the difference in hybridization between DNA duplexes on the surface versus those in solution. However, duplex kinetics on ssDNA chips are heterogeneous hybridization consisting of many kinetic coefficients of reversible nonspecific adsorption and desorption of the targets with the probes in various random conformations. These different approaches individually and collectively have provided new insight of the complexity in DNA hybridization kinetics on

surfaces. However, the actual kinetics of DNA duplex formation in complex milieu has only been considered conceptually by a combination of various approaches addressed individually, without a global method to accurately and reilably predict in such complex multi-equilibria systems.[218] Experimental data to validate duplex models for short, well-controlled ssDNA immobilized layers as a function of controlled media and controlled densities are not yet available.

Additionally, both Moiseev et al.[128] and Unruh et al.[219] reported the influence of dye-DNA interactions, using fluorescence methods to study biomolecular dynamics under fluorescent dye influences on chain mobility and conformation with labeled ssDNA. Dye-labeled ssDNA influences the chain conformation and length both before and after hybridization with dye-labeled and unlabeled targets, thereby affecting hybridization kinetics and efficiency.[219] As DNA hybridization is a complex 3D scenario that must consider various factors including non-specific binding, transport of target from bulk to crowded, charged probe surfaces, variable probe densities, competitive binding, and secondary structural issues, the time to attain equilibrium in such complex situations is not readily predictable. The result is that most actual assays cannot readily know when an equilibrium endpoint is achieved for each assay. Assays that terminate before equilibrium is reached could produce an inaccurate answer.[203, 204, 212] Experimental designs including microfluidic, statistical modeling and simulation approaches should be considered to understand the kinetics of real time hybridization in microarrays in complex milieu for efficient endpoint analysis.

10. Use of probe linker chemistry as spacers in ssDNA probe surface immobilization

Surface immobilization technologies have long exploited spacer chemistries to enhance bio-affinity interactions at surfaces.[220] Flexible spacer chemistries (e.g., oligoethylene glycols, reactive alkanes, oligo(dT) tails), are frequently utilized on probe termini as an alternative anchoring chemistry to direct ssDNA probe surface coupling (typically a hexamethylene anchoring spacer with functional coupling group) in order to improve DNA probe immobilization quality and enhance their hybridization capabilities in microarrays. [221]. These immobilizing spacers are highly diverse both chemically and physically, and can include various nucleotide or hydrophilic synthetic oligomers with diverse claims to their effects on hybridization yields. Low ssDNA probe grafting densities allow probes to lie flat on the solid surface, reducing accessible ssDNA probe chain configurations. Higher grafting densities yield different ssDNA brush regimes (see Figure 4) that introduce hybridization penalties in both steric and electrostatic forms (*vida supra*). Hence, long flexible spacers weaken probe-surface effects, and their hybridization behavior can approach more bulk-like characteristics, depending on media effects (ionic strength) that affect ssDNA mobility and mechanics (*vida surpa*).[111] Probe brush or mushroom regimes can be formed on surfaces when ssDNA is tethered with spacers, depending on the number of bases in the probe and the spacer length. However, this effect also depends strongly on ssDNA target length.[37] A unique probe brush regime was reported for long neutral spacers (e.g., ethylene glycol oligomers) and short targets at intermediate media ionic strengths

where ssDNA chain stretching in response to local electrostatic interactions between immobilized probes is facilitated.[111] In contrast to the advantages of relieving steric issues at the grafting site, a non-monotonic effect of spacer length is observed when targets are short. At higher grafting densities, probe chains crowd each other, producing a polymer brush, higher ssDNA surface charge density, possible Coulombic blockage, steric hindrance to approaching targets and resulting poor duplex efficiency.[111]

11. Hairpin and secondary structured probes in arrays

Assessing control of probe density on substrates to optimize further probe-target binding kinetics in microarray applications is important in conventional linear oligomer ssDNA arrays. However, with the advent of deliberately structured next-generation probe sensors, such as those incorporating designer secondary structures such as hairpins as in molecular beacons or aptamers,[222, 223] it becomes more important to understand these surface-mediated structural effects on array polymer layer properties, assay kinetics and answers. These looped immobilized probes are deliberately designed with meta-stable folded immobilized states triggered to change conformation in the presence of complementary target.[221] Intramolecular base pairs involved in secondary structure that stabilize single-stranded self-conformations create a higher energy barrier to intermolecular hybridization, altering hybridization kinetics. Additionally, the more dramatic conformational changes required to open a hairpin loop require different surface spatial characteristics than linear probes to permit accessibility to incoming target required to trigger the transformation. Comparative studies of DNA hybridization kinetics both in solution and on the surface with SPR, UV absorbance, QCM indicate that both probe and target secondary structure affect hybridization kinetics.[222] Although planar gold surfaces and conventional ssDNA probe layer environments suppress the measured duplex rates 20- to 40- fold compared to their bulk behaviors, the effects of secondary structure produce similar duplex behaviors in solution versus surface environments.[222]

ssDNA probes deliberately designed to contain secondary structures such as hairpin loops (e.g., molecular beacons) alter their spatial requirements, probe immobilization densities and chain physics on surfaces with subsequent effects on hybridization in microarray assays.[224–226] The role of the surface in ssDNA folding is more complicated than simply restricting conformations available to the random coil state.[227] Some molecular beacon probe designs enable separation from the surface to minimize surface influences.[228] Several known molecular motifs alter ssDNA secondary structures thereby influencing the thermodynamics and kinetics of hybridization reactions.[229] Both ssDNA probe and stem lengths impact hairpin probe binding specificity and hybridization rates.[230] Their stem-loop structure provides a competing reaction for probe-target hybridization that serves to increase probe specificity, and is particularly useful when single-base discrimination is desired.[231] Probe hairpin stem base composition and overall loop length significantly affect their sensitivity and selectivity: surface-immobilized hairpins discriminated between two sequences differing by a single base-pair mismatch with high sensitivity (>order of magnitude difference in signal).[232] Thermodynamic analysis of the transitions between open-closed hairpin loop states justifies their improved specificity. Structural constraints on probe loop conformations lead to enhanced specificity with increasing stem length,

increasing the difference between melting temperatures of perfectly complementary duplexes and mismatched duplexes.[233] Rates of spontaneous hairpin self-duplex formation may be reduced by decreasing loop length and increasing stem length.[234] Aalberts et al.[235] showed that the persistence length for beacon-type hairpin loops depends on their base stacking enthalpy, stacking entropy and temperature. Stacking also plays an important role in the kinetic behavior and folding conformations of these hairpins in solution. As temperature decreases, stacked regions become longer and loop closing times increase. Open/closed hairpin transition rates are reported in microsecond range.[236]

Gao et al.[222] showed that hairpins with longer stem lengths have improved abilities to discriminate between targets over broader ranges of temperatures. However, this is accompanied by decreased hybridization rates. Longer hairpin probe lengths tend to have lower dissociation constants, increased kinetic rate constants, and reduced specificity. Consistently, very short stems exhibit lower signal-to-background ratios than longer stems. Yao et al[234] studied the hybridization kinetics of surface-immobilized single-molecule hairpin beacon-type probes. Hybridization produces a spontaneous conformational reorganization with the stem opening, leading to fluorescence restoration. Du et al.[232] found that hybridization efficiency is sensitive both to hairpin secondary structure immobilized on gold surfaces, as well as to DNA hairpin immobilized density. Kastantin et al. [237] found that ssDNA hairpins exhibit faster kinetics on hydrophobic (trimethylsliane) versus hydrophilic (OEG) surfaces: TMS is claimed to favor hairpin states both by slowing ssDNA unfolding and speeding up folding relative to OEG. Yao et al.[234] investigated biotinylated ssDNA hairpin probes immobilized on avidin surfaces. A 25-base linker was found optimal for hybridization.

12. DNA probe printing and drying produces immobilized DNA heterogeneity

ssDNA probes on many commercial and home-brew arrays are deposited on substrates (e.g., reactive, coated glass substrates) by spatially controlled deposition of nanoliter drops of complex ssDNA solutions using robotic spotters, followed by evaporation of deposited liquid droplets within seconds.[86, 238] Non-contact inkjet printing and contact (pin) spotting of DNA generally all yield sub-microliter droplet volumes on surfaces as the basis for ssDNA microspot formation in arraying. Unfortunately, droplet drying at this size scale and with typical arraying conditions most frequently results in inhomogeneous solute deposition upon droplet drying.[39, 238] For assay purposes, this resulting ssDNA dried spot heterogeneity is undesired, but is difficult to control from the combined phenomena of droplet solution composition, deposition wetting, spreading, evaporation, and subsequent ssDNA drying patterns. Evaporation from sessile droplets induces radial convection within the drop, producing the well-known “coffee ring” drying effect.[239, 240] Deegan et al. [241] pointed out that the physical origin of the coffee stain effect is due to a combination of pinning of the three-phase contact line and a convective flux driven by the evaporation. The occurrence of “coffee stain like” droplets is caused by a combination of solvent evaporation and contact line pinning: whenever the contact line of an evaporating drop is prevented from receding, a convective flux is generated from the center towards the edge of the drop in

order to sustain the solvent evaporation.[242] This flux carries solute from the bulk of the drop towards the contact line, leading to a local increase in concentration and eventually to precipitation of the solute at the drying droplet edges.

Droplet evaporation also induces a gradient in temperature across the droplet and consequently a gradient in surface tension, generating Marangoni flow.[86] In a sessile evaporating drop, Marangoni stress (i.e., a surface tension gradient over the droplet during evaporation) can be induced by local temperature variation near the fluid interface or by change in concentration caused by solvent evaporation.[239] The circulating convective flows lead to intensive mixing of the solutes during evaporation, helping to overcome mass transport limitations due to the coffee ring effect. Marangoni droplet drying patterns with high concentration of the ssDNA at the dried droplet center are the result.[243, 244] Drying conditions for printed ssDNA droplets on a surface are proposed to result from competition between the dominant effects of coffee ring versus Marangoni droplet drying patterns.[34] Dugas et al.[86] studied the effect of ssDNA droplet drying on hydrophobic flat surfaces and proposed that droplets flatten with a constant contact area, and then the droplet shrinks at a constant contact angle. These results produce variations in diameters and morphologies for thousands of spots deposited on microarray surfaces that are not uniform since their local wetting/spreading and resulting drying behaviors are non-uniform from sub-micron variabilities in solid support chemistry. If surfaces exhibit sufficiently uniform chemistry, then control of some physicochemical properties (wetting, evaporation rate) of the droplet allows formation of well-controlled spots compatible with ssDNA grafting.

Overall, the rapid evaporative process produces increased solution ionic strength and solute concentrations in the drying ssDNA film, resulting in distinct differences in immobilized ssDNA structure, density and chemistry compared to bulk solution coupling reactions between ssDNA and surfaces.[245] Probe spot drying thus commonly leads to “halo” or “doughnut” shaped spots which provide variable integrated intensities and target capture with conventional fluorescence scanner readings. Extensive high-resolution imaging techniques such as confocal epifluorescence can be combined with other more exotic surface analytical tools (e.g., TOF-SIMS and XPS compositional surface imaging) to evaluate the chemical distribution of ssDNA within dried spots and probe effects due to drying artifacts. [34, 86, 246]. The major significance of probe spot drying is that each probe ssDNA is deposited in highly heterogeneous densities across any given spot, and none reproducibly. Since ssDNA probe density is a primary determinant of target capture (*vida supr*a), arrays then capture targets with different kinetics and efficiencies depending on local probe densities that remain uncontrolled by printing methods. This produces substantial variations in signals from spots, both spatially within spots and spot-spot. Integrated signal intensities, representing common spot assay “answers” then depend on local drying phenomena and not necessarily on the ideal strand duplex characteristics based on complementarity.

Pappaert et al.[247] reported hybridization processes as a primary cause of doughnut-shaped ssDNA spot images used to determine assay signals. A combination of computer simulation, theoretical calculation and optical technique measurements have shown that the ring-shaped hybridization pattern results from diffusion-limited conditions present during hybridization process.[29] Near spot centers, ssDNA target is delivered to the probe surface solely through

linear normal diffusion, whereas toward the outer edge, a lateral (radial) component of diffusive flux augments the normal linear transport component, producing hemispherical diffusion. This results in spot outer edges accumulating more target through greater proximate fluid volume transport versus spot centers.[33] Since equilibrium binding depends on many factors in multiplexed arrays (*vida supra*), determining equilibrium duplex binding for each spot when many probe and target strand sequences are present is difficult. These authors therefore hypothesized that these spot patterns occur during hybridization, especially with short oligonucleotides that have a very high binding probability and fast hybridization kinetics. Longer target ssDNA molecules and long assay times lead to a more evenly distributed intensity signals. Studies by Dandy et al. indicate that near the spot center, target is delivered to the probe surface solely through the linear normal diffusion component whereas toward the outer edge, a lateral (radial) component of diffusive flux augments the normal linear transport component, producing hemispherical diffusion.[29] These effects result collectively in the outer spot edges accumulating more ssDNA targets through sampling greater proximate fluid volume transport versus spot centers. This was further verified by real-time hybridization kinetics studies using imaging with confocal fluorescence microscopy.[33]

Assay signal answer is therefore a multi-factorial result of the influence of high probe density heterogeneity upon droplet drying[33, 34] on duplex formation, combined with intrinsic target mass transport effects from target concentrations and other known kinetic influences of various probe-target combinations that produce both cross-hybridized mismatches and perfect matches in competition at surfaces.[29, 218] Improving the uniformity of probe coverage across each spot feature could improve assay signal consistency at any given assay endpoint, even prior to target saturation at the unique equilibrium point for any given spot probe-target pairing.

Further details of dried intra-spot and spot-to-spot heterogeneity seen with different concentrations of both total DNA and fraction of dye-labeled ssDNA can be explained from spot drying behavior in the presence of ssDNA-bound signal dyes, surfactants and dissolved salts.[86, 143] Evaporation kinetics and behaviors for droplets containing ssDNA varied as a function of ssDNA concentration: drops containing very low ssDNA concentrations dried by maintaining a constant base area (pinning),[85] whereas those with high concentration dried with a constant contact angle. Fang et al.[85] showed with confocal and rheological studies that high concentration ssDNA droplets formed a shell while low ssDNA concentrations resulted in isolated island formation. Various efforts to improve inter-spot ssDNA dried spot such as increased relative humidity from 40% to 80% during drying and also use of surfactants such as betaine and co-solvents like DMSO. McQuain et al.[248] optimized surfactant concentration to 1.5M betaine and maintained relative humidity at 60%, reducing inter-spot and intra-spot variations. Addition of anionic surfactant (e.g., SDS) initially facilitates uniform droplet spreading and stabilizes the drop evaporation, drastically altering the “coffee ring effect”.[249] Surfactant-driven Marangoni flows arise when the local surfactant concentration at the pinned contact line increases due to the coffee ring effect, thereby decreasing the local surface tension and inducing Marangoni flow towards the spot center.[239] The extent of circular Marangoni flow is influenced by variation of SDS

concentration along the air-water interface.[249] Spot evaporation modes can also be influenced by salts, with DNA probe deposition patterns following the salting trace.[86] Schematics of ssDNA droplet drying in the presence of solutes, salts and buffers, leading to either coffee-ring or Marangoni droplet drying phenomena, are shown in Figure 8.

Phase separation upon drying, producing salt crystallization in evaporating droplets of ssDNA solutions containing salts, occurs as well.[250, 251] Exceeding the local solubility limit for different salts in evaporating droplets leads to rich morphologies of deposited salt crystals and ssDNA. Formation of radially varying salt concentration yields deposited rings with spacing between the concentric rings that depends on the ssDNA concentration and ion species concentration.[251] Marangoni inward flow of solution produces various salt patterns with deposition of the ssDNA-dye in concentric patterns within spots.[252] The physicochemical properties of the evaporating ssDNA solution are influenced by the dynamic changes in ssDNA concentration, changing ionic strength and surfactant concentrations, influencing final dried ssDNA patterns.[86] Theoretical and experimental results conclude that at low concentrations of salt, the deposit becomes more uniform, covering the entire surface beneath the droplet, whereas at higher concentration, salt deposits appear predominantly along the outer rim of the spot.[251] At lower ssDNA concentration, ssDNA at the liquid-vapor interface is deposited at the droplet edge during initial evaporation stages, and eventually under developing Marangoni flow, transitions to deposition of ssDNA aggregates at the spot centers. Hence, periodic patterning is less dominant at very low concentrations due to reduced spreading. Nonetheless, drying of many ssDNA droplets containing mixtures of ssDNA, surfactants and dissolved salts undergo phase separation. Despite the use of non-ionic/zwitterionic surfactants to limit ssDNA probe interactions, ssDNA segregation[86] into two phases can occur upon drying: one enriched in ssDNA and another in surfactant, leading to another form of phase segregation upon drying and formation of a ssDNA precipitate with increasing electrolyte and surfactant concentration upon evaporation.[252–254] Furthermore, supersaturated salt conditions also promote ssDNA phase separation.[86, 251] Precipitation occurs at very low concentrations of both ssDNA and surfactant, and is further enhanced in the presence of electrolytes.[246, 254–256] Similar aggregation is predominant at higher ssDNA concentrations (i.e., micromolar to molar)[82] and with dye labeled ssDNA oligomers.[83] It is likely that such concentrations are achieved within the droplets within a few seconds of printing due to rapid drying.

Furthermore, cyanine dyes analogous to commonly used ssDNA label Cy-3 are known to readily form molecular aggregates in aqueous media.[257] Cyanine dyes are also known to interact with dsDNA in aqueous media through various interactions, either by intercalation, minor groove binding between base pairs or dye-dye aggregation.[82, 257, 258] Cyanine dye aggregation is also reported in Langmuir-Blodgett monolayer of amphiphilic nucleic acids during evaporation rates controlled by mass transfer across the aqueous-film-air interface.[259] In cyanine dye-labeled single-strand probe ssDNA, dye–dye interactions and dye–nucleotide aggregations in the presence of increasing ionic strength and surfactant concentrations reduce probe stability and quench fluorescence.[83, 124, 219] Singly labeled fluorescent ssDNA probes exhibit dye–ssDNA interactions as studied by fluorescence anisotropy and lifetime assays. As Cy3-ssDNA content increases in print solutions up to

100% ssDNA mass fraction, ssDNA aggregation is seen to be much more predominant leading to increasing dye quenching and reducing fluorescence intensity.[34]

As these various factors affect droplet drying morphology, including ssDNA concentration, temperature, humidity, buffer, salts and dye-labels, in complex ways, efforts to alter microdroplet footprint shapes on surfaces have recently gained attention. Yunker et al[242]. and Weon et al.[243] altered droplet shapes to obtain uniform droplet drying. Additionally, polymer “lift-off” arrays combine the hydrophobic surface properties of di-p-xylylene (Parylene) with photolithographically etched hydrophilic openings within the polymer substrate to control spot morphology[260] and resulting uniformity of deposition.[261] Manipulating surface wetting properties, mixing of the droplet with frequency dependent oscillating flow[262] to alter flow pattern of the evaporating droplet, and electrowetting[263] -driven microfluidic flows are shown to suppress coffee ring effects for variable concentrations. The global objective of these strategies is to modify and perhaps control DNA probe deposition physics on surfaces, specifically to affect probe immobilization density and lateral distributions within dried DNA spots that affect assay equilibrium and reliable assay ‘answers’.

13. Conclusions

DNA microarrays have been used extensively for more than a decade in numerous forms. However, high variabilities in the designs and applications of probes, surfaces, targets and types of immobilization (different platforms) has led to challenges in obtaining reproducible and reliable assay results. This is particularly challenging in those that produce assay answers directly from complex samples without PCR amplification, or whose signals seek to reflect target absolute abundance (i.e., quantitative output). The coordinated probe and substrate design techniques for “grafting to”, and “grafting from” ssDNA probes, challenges in overcoming kinetic limitations of assay in multiplex mode and in dense probe states, and variations caused by spot deposition methods have compelling limitations in attaining uniform ssDNA probe grafting efficiency and probe density, and reliable target capture. These result in microarrays with deficiencies in the resulting assay metrics, reproducibility and reliability as a diagnostic format.

The biophysical aspects of ssDNA molecular mechanics, conformations, electrostatics, control and stability of surface-tethered states, interactions with the surface, with neighboring probes, with matched and mismatched targets in competition, and within high ionic strength environments in duplex formation all impact the array behavior and assay answer. These factors have been subject to some study in simplified formats. *However, none have been studied in relevant combinations present in real nucleic acid-based assays.*

To improve these assays, these variables need to be more thoroughly evaluated in surface-immobilized formats since there is no direct translation of bulk ssDNA characteristics to surface-tethered ssDNA properties. Common polymer physical parameters such as radius of gyration, persistence length, ssDNA elasticity, flexibility and chain conformational mechanics have not been investigated in detail for either surface-tethered ssDNA or dsDNA. ssDNA probe chain accessibility on surfaces that determines target binding and ultimately

array performance is determined by local tethered flexibility and conformations based on ssDNA sequence, electrostatic interactions, media influences, substrate chemistry and surface immobilization techniques. Though various theoretical and experimental approaches seek to explain DNA surface behavior with optical, fluorescent, and force spectroscopies, several discrepancies persist for explaining ssDNA flexibility vs. stiffness at surfaces. ssDNA chain conformations effects due to phosphate backbone charges and base stacking are still unresolved. WLC remains the widely accepted classic model for understanding ssDNA molecular mechanics despite its several shortcomings. Extensive improvements have been made to the WLC model to accommodate ssDNA bending angles and chain flexibility. Various molecular dynamics simulations and other models have been developed to attempt to correlate and supplement the shortcomings of WLC. The newly developed coarse-grained approach is widely accepted for treating ssDNA as an inextensible elastic rod and despite lacking atomic details, is accurate for thousands of base pairs down to few hundred. However, its applicability remains controversial for short DNA molecules with persistence lengths of less than 1nm, and remains unvalidated as a function of the many variables used in experimental array assays.

Studies of physical structure and biophysical properties of ssDNA as well as mechanistic extensions to short immobilized ssDNA probes at surfaces have proven useful in initial understanding of some fundamental issues relevant to nucleic acid capture at surfaces. Modeling and simulations contribute to explaining these data but are limited when dealing with short, rigid polyelectrolyte DNA probe chains at surfaces in complex ionic milieu. The process of DNA hybridization at surfaces is a critical part of nucleic acid-based array technology; fundamental understanding of this process under relevant conditions for actual assays is very challenging currently. Future improvements in the development and fabrication of microarrays, designing new nucleic acid applications, will require better knowledge of ssDNA as tethered chains and how strand-strand duplexation behavior is controlled kinetically and thermodynamically under assay conditions that approach equilibrium slowly in complex media. Comparisons of actual assay conditions experienced by tethered DNA probes on array surfaces versus current capabilities to model DNA brushes using scaling theories are summarized in Table 3.

The complexity of this task is compounded by the large number of reported protocols for preparing and functionalizing surfaces for DNA microarray use in practical assay deployment and in the various milieu these assays are conducted. Polyelectrolyte media and interfacial brush as well as aqueous droplet drying theories help to elucidate some basic properties of ssDNA target-probe interactions, media and substrate effects. These provide additional information to analyze the effects of immobilized ssDNA probe density on the thermodynamics and kinetics of DNA hybridization on array surfaces in simple binary and even multiplex assay modes. As the kinetics and thermodynamics of immobilized probe molecules tethered farther away from the solid support can approach those in solution states, the utility of introducing spacer chains for ssDNA immobilization is currently exploited but largely from an empirical approach. The beneficial role of spacers is generally recognized, but a coherent view of their optimal design and underlying physics has not been presented. Accurate measurement of probe surface coverage, a parameter crucial for determination of efficiencies of immobilization and hybridization protocols, is extremely difficult. More

careful evaluation of probe lateral density and its heterogeneity for understanding this influence on target hybridization isotherms and rate constants for different platforms are required to understand DNA microarray performance. Clear elucidation of molecular mechanisms surrounding DNA duplex formation on tethered probe surfaces and sources of its variability will move the nucleic acid microarray approach to standardization, and even toward rigorous quantitative answers required for their more successful clinical translation to inform medical decision-making.

Acknowledgments

This work was supported by NIH grant R01 EB001473.

List of Abbreviations

$\mathbf{L_p}$	persistence length
$\boldsymbol{\kappa^{-1}}$	Debye length
$\mathbf{l_B}$	Bjerrum length
$\mathbf{R_g}$	radius of gyration
$\mathbf{N_{av}}$	Avogadro's number
$\mathbf{R_F}$	Flory radius of the free chain
N	number of DNA nucleotide/base (length of DNA/polymer chain)
L	DNA chain length, D, lateral chain spacing
b	nucleotide size
Z	ionic strength
K	Boltzmann constant
T	temperature
$\mathbf{c_s}$	salt concentration
m	the number of neutral (uncharged) monomer units in the chain between two neighboring charged monomers
a	the monomer unit length (0.3–0.6nm)
H	osmotic brush thickness
$\mathbf{L_{Pi}}$	bare persistence length
$\mathbf{L_{Pe}}$	electrostatic persistence length
$\mathbf{L_{pa}}$	apparent persistence length
θ	angle of semiflexible polymer
σ	probe surface density or chain grafting density
ρ(z)	chain segment distribution

n	the number of segments attached to it by one of its ends at a tethered surface density of σ
z	distance from the substrate
ν	Flory scaling exponent
ξ	neutralization length (Gouy-Chapman length)
H	DNA probe brush thickness
x	counterion cloud thickness
Σ_0	surface area of probe
K_E	equilibrium constant
k_f	rate of forward reaction
k_r	rate of reverse reaction

References

1. Heller, MJ. DNA microarray technology: Devices, systems, and applications. 2002. p. 129-53.
2. Hoheisel JD. Microarray technology: Beyond transcript profiling and genotype analysis. Nature Reviews Genetics. 2006; 7:200–10.
3. Bulyk ML. DNA microarray technologies for measuring protein-DNA interactions. Current Opinion in Biotechnology. 2006; 17:422–30. [PubMed: 16839757]
4. Gresham D, Dunham MJ, Botstein D. Comparing whole genomes using DNA microarrays. Nature Reviews Genetics. 2008; 9:291–302.
5. Evans WE, Relling MV. Moving towards individualized medicine with pharmacogenomics. Nature. 2004; 429:464–8. [PubMed: 15164072]
6. Bryant PA, Venter D, Robins-Browne R, Curtis N. Chips with everything: DNA microarrays in infectious diseases. Lancet Infectious Diseases. 2004; 4:100–11. [PubMed: 14871635]
7. Kononen J, Bubendorf L, Kallioniemi A, Bärlund M, Schraml P, Leighton S, et al. Tissue microarrays for high-throughput molecular profiling of tumor specimens. Nature Medicine. 1998; 4:844–7.
8. Sobrino B, Brión M, Carracedo A. SNPs in forensic genetics: A review on SNP typing methodologies. Forensic Science International. 2005; 154:181–94. [PubMed: 16182964]
9. Lobenhofer EK, Bushel PR, Afshari CA, Hamadeh HK. Progress in the application of DNA microarrays. Environmental Health Perspectives. 2001; 109:881–92. [PubMed: 11673116]
10. Stears RL, Martinsky T, Schena M. Trends in microarray analysis. Nature Medicine. 2003; 9:140–5.
11. Pusztai L. Chips to bedside: Incorporation of microarray data into clinical practice. Clinical Cancer Research. 2006; 12:7209–14. [PubMed: 17189391]
12. Li X, Quigg RJ, Zhou J, Gu W, Nagesh Rao P, Reed EF. Clinical utility of microarrays: Current status, existing challenges and future outlook. Current Genomics. 2008; 9:466–74. [PubMed: 19506735]
13. Shi L. The MicroArray Quality Control (MAQC) project shows inter- and intraplatform reproducibility of gene expression measurements. Nature Biotechnology. 2006; 24:1151–61.
14. Ji H, Davis RW. Data quality in genomics and microarrays. Nature Biotechnology. 2006; 24:1112–3.
15. Lundeberg J, Klevebring D, Gry M, Lindberg J, Eidefors A. Automation of cDNA synthesis and labelling improves reproducibility. Journal of Biomedicine and Biotechnology. 2009; 2009

16. Šášik R, Woelk CH, Corbeil J. Microarray truths and consequences. Journal of Molecular Endocrinology. 2004; 33:1–9. [PubMed: 15291738]

17. Tseng GC, Oh MK, Rohlin L, Liao JC, Wong WH. Issues in cDNA microarray analysis: Quality filtering, channel normalization, models of variations and assessment of gene effects. Nucleic Acids Research. 2001; 29:2549–57. [PubMed: 11410663]

18. Hess KR, Zhang W, Baggerly KA, Stivers DN, Coombes KR, Zhang W. Microarrays: Handling the deluge of data and extracting reliable information. Trends in Biotechnology. 2001; 19:463–8. [PubMed: 11602311]

19. Peters JP, Maher LJ. DNA curvature and flexibility in vitro and in vivo. Quarterly Reviews of Biophysics. 2010; 43:23–63. [PubMed: 20478077]

20. Schena, M. Microarray analysis. Wiley-Liss; Hoboken, NJ: 2003.

21. Barbulovic-Nad I, Lucente M, Sun Y, Zhang M, Wheeler AR, Bussmann M. Bio-microarray fabrication techniques - A review. Critical Reviews in Biotechnology. 2006; 26:237–59. [PubMed: 17095434]

22. Gong, P.; Grainger, DW. Microarrays: Methods in Molecular Biology-Methods and Protocols. 2007.

23. Duggan DJ, Bittner M, Chen Y, Meltzer P, Trent JM. Expression profiling using cDNA microarrays. Nature Genetics. 1999; 21:10–4. [PubMed: 9915494]

24. Wu P, Castner DG, Grainger DW. Diagnostic devices as biomaterials: A review of nucleic acid and protein microarray surface performance issues. Journal of Biomaterials Science, Polymer Edition. 2008; 19:725–53. [PubMed: 18534094]

25. Sassolas A, Leca-Bouvier BD, Blum LJ. DNA biosensors and microarrays. Chemical Reviews. 2008; 108:109–39. [PubMed: 18095717]

26. Schena M, Heller RA, Theriault TP, Konrad K, Lachenmeier E, Davis RW. Microarrays: Biotechnology's discovery platform for functional genomics. Trends in Biotechnology. 1998; 16:301–6. [PubMed: 9675914]

27. Chowdhury, EH.; Akaike, T. Case studies-Development of oligonucleotides. Cary, North Carolina: Wiley-interscience; 2007.

28. Lausted C, Dahl T, Warren C, King K, Smith K, Johnson M, et al. POSaM: a fast, flexible, open-source, inkjet oligonucleotide synthesizer and microarrayer. Genome Biology. 2004; 5:R58–R. [PubMed: 15287980]

29. Dandy DS, Wu P, Grainger DW. Array feature size influences nucleic acid surface capture in DNA microarrays. Proc Natl Acad Sci U S A. 2007; 104:8223–8. [PubMed: 17485675]

30. Peterson AW, Heaton RJ, Georgiadis RM. The effect of surface probe density on DNA hybridization. Nucleic Acids Res. 2001; 29:5163–8. [PubMed: 11812850]

31. Liu RH, Yang J, Lenigk R, Bonanno J, Grodzinski P. Self-Contained, Fully Integrated Biochip for Sample Preparation, Polymerase Chain Reaction Amplification, and DNA Microarray Detection. Analytical Chemistry. 2004; 76:1824–31. [PubMed: 15053639]

32. Gong P, Grainger DW. Comparison of DNA immobilization efficiency on new and regenerated commercial amine-reactive polymer microarray surfaces. Surface Science. 2004; 570:67–77.

33. Rao AN, Rodesch CK, Grainger DW. Real-Time Fluorescent Image Analysis of DNA Spot Hybridization Kinetics To Assess Microarray Spot Heterogeneity. Analytical Chemistry. 2012; 84:9379–87. [PubMed: 23043216]

34. Rao AN, Vandencasteele N, Gamble LJ, Grainger DW. High-resolution epifluorescence and time-of-flight secondary ion mass spectrometry chemical imaging comparisons of single DNA microarray spots. Analytical Chemistry. 2012; 84:10628–36. [PubMed: 23150996]

35. Ramakrishnan R, Dorris D, Lublinsky A, Nguyen A, Domanus M, Prokhorova A, et al. An assessment of Motorola CodeLink microarray performance for gene expression profiling applications. Nucleic Acids Research. 2002:30.

36. Dai H, Meyer M, Stepaniants S, Ziman M, Stoughton R. Use of hybridization kinetics for differentiating specific from non-specific binding to oligonucleotide microarrays. Nucleic Acids Research. 2002:30.

37. Halperin A, Buhot A, Zhulina EB. On the hybridization isotherms of DNA microarrays: The Langmuir model and its extensions. Journal of Physics Condensed Matter. 2006; 18:S463–S90.

38. Gong P, Lee CY, Gamble LJ, Castner DG, Grainger DW. Hybridization behavior of mixed DNA/alkylthiol monolayers on gold: Characterization by surface plasmon resonance and 32P radiometric assay. Analytical Chemistry. 2006; 78:3326–34. [PubMed: 16689533]
39. Venkatasubbarao S. Microarrays--status and prospects. Trends in Biotechnology. 2004; 22:630–7. [PubMed: 15542153]
40. Conti M, Bustanji Y, Falini G, Ferruti P, Stefoni S, Samorì B. The desorption process of macromolecules adsorbed on interfaces: The force spectroscopy approach. ChemPhysChem. 2001; 2:610–3. [PubMed: 23686879]
41. Paleček E. Electrochemical behaviour of biological macromolecules. Bioelectrochemistry and Bioenergetics. 1986; 15:275–95.
42. Lee CY, Gong P, Harbers GM, Grainger DW, Castner DG, Gamble LJ. Surface coverage and structure of mixed DNA/Alkylthiol monolayers on gold: Characterization by XPS, NEXAFS, and fluorescence intensity measurements. Analytical Chemistry. 2006; 78:3316–25. [PubMed: 16689532]
43. Lee C-Y, Gamble LJ, Grainger DW, Castner DG. Mixed DNA/oligo (ethylene glycol) functionalized gold surfaces improve DNA hybridization in complex media. Biointerphases. 2006; 1:82–92. [PubMed: 20408620]
44. Lee C-Y, Nguyen P-CT, Grainger DW, Gamble LJ, Castner DG. Structure and DNA hybridization properties of mixed nucleic acid/maleimide-ethylene glycol monolayers. Analytical Chemistry. 2007; 79:4390–400. [PubMed: 17492838]
45. Dias RS, Pais AACC, Linse P, Miguel MG, Lindman B. Polyion adsorption onto catanionic surfaces. A Monte Carlo study. Journal of Physical Chemistry B. 2005; 109:11781–8.
46. Stillman BA, Tonkinson JL. FAST(TM) slides: A novel surface for microarrays. BioTechniques. 2000; 29:630–5. [PubMed: 10997277]
47. Grainger, DW.; Greef, CH.; Gong, P.; Lochhead, MJ. Current Microarray Surface chemistry. In: Rampal, JB., editor. Microarrays Volume-1 Synthesis Methods. Humana Press; 2007. p. 37-58.
48. Araki S, Nakai T, Hizume K, Takeyasu K, Yoshikawa K. Hydrodynamic radius of circular DNA is larger than that of linear DNA. Chemical Physics Letters. 2006; 418:255–9.
49. Flory, JP. Principles of polymer chemistry. Cornell University Press; 1953.
50. Currie E, Norde W, Cohen Stuart M. Tethered polymer chains: surface chemistry and their impact on colloidal and surface properties. Advances in colloid and interface science. 2003; 100:205–65. [PubMed: 12668330]
51. Halperin A, Buhot A, Zhulina EB. Brush effects on DNA chips: Thermodynamics, kinetics, and design guidelines. Biophysical Journal. 2005; 89:796–811. [PubMed: 15908581]
52. Moh LC, Losego MD, Braun PV. Solvent Quality Effects on Scaling Behavior of Poly (methyl methacrylate) Brushes in the Moderate-and High-Density Regimes. Langmuir. 2011; 27:3698–702. [PubMed: 21401067]
53. De Gennes, P-Gd; Pincus, P.; Velasco, R.; Brochard, F. Remarks on polyelectrolyte conformation. Journal de physique. 1976; 37:1461–73.
54. Zhulina EB, Borisov OV, Priamitsyn VA. Theory of steric stabilization of colloid dispersions by grafted polymers. Journal of Colloid and Interface Science. 1990; 137:495–511.
55. Birshtein T, Liatskaya YV, Zhulina E. Theory of supermolecular structures of polydisperse block copolymers: 1. Planar layers of grafted chains. Polymer. 1990; 31:2185–96.
56. Wijmans C, Scheutjens J, Zhulina E. Self-consistent field theories for polymer brushes: lattice calculations and an asymptotic analytical description. Macromolecules. 1992; 25:2657–65.
57. Milner ST. Strong-stretching and Scheutjens–Fleer descriptions of grafted polymer brushes. J Chem Soc, Faraday Trans. 1990; 86:1349–53.
58. Currie E, Leermakers F, Cohen Stuart M, Fleer G. Grafted adsorbing polymers: scaling behavior and phase transitions. Macromolecules. 1999; 32:487–98.
59. Bracha D, Karzbrun E, Shemer G, Pincus PA, Bar-Ziv RH. Entropy-driven collective interactions in DNA brushes on a biochip. Proceedings of the National Academy of Sciences. 2013; 110:4534–8.

60. Zhulina EB, Rubinstein M. Ionic strength dependence of polyelectrolyte brush thickness. Soft Matter. 2012; 8:9376–83. [PubMed: 23144649]
61. Bijsterbosch H, De Haan V, De Graaf A, Mellema M, Leermakers F, Stuart MC, et al. Tethered adsorbing chains: neutron reflectivity and surface pressure of spread diblock copolymer monolayers. Langmuir. 1995; 11:4467–73.
62. Fleer, GJ. Polymers at interfaces. Springer; 1993.
63. Kumar NA, Seidel C. Polyelectrolyte brushes with added salt. Macromolecules. 2005; 38:9341–50.
64. Hariharan R, Biver C, Mays J, Russel W. Ionic strength and curvature effects in flat and highly curved polyelectrolyte brushes. Macromolecules. 1998; 31:7506–13.
65. Hariharan R, Biver C, Russel W. Ionic strength effects in polyelectrolyte brushes: The counterion correction. Macromolecules. 1998; 31:7514–8.
66. Pryamitsyn V, Leermakers F, Zhulina E. Brush theory of tethered chains with a charged group at the free end. Macromolecules. 1997; 30:584–9.
67. Borisov O, Leermakers F, Fleer G, Zhulina E. Polyelectrolytes tethered to a similarly charged surface. The Journal of Chemical Physics. 2001; 114:7700.
68. Zhulina E, Klein Wolterink J, Borisov O. Screening effects in a polyelectrolyte brush: self-consistent-field theory. Macromolecules. 2000; 33:4945–53.
69. Israels R, Leermakers F, Fleer G. On the theory of grafted weak polyacids. Macromolecules. 1994; 27:3087–93.
70. Lyatskaya YV, Leermakers F, Fleer G, Zhulina E, Birshtein T. Analytical self-consistent-field model of weak polyacid brushes. Macromolecules. 1995; 28:3562–9.
71. Manning GS. Limiting laws and counterion condensation in polyelectrolyte solutions I. Colligative properties. Journal of Chemical Physics. 1969; 51:924–33.
72. Zhulina E, Birshtein T, Borisov O. Theory of ionizable polymer brushes. Macromolecules. 1995; 28:1491–9.
73. Gong P, Levicky R. DNA surface hybridization regimes. Proc Natl Acad Sci U S A. 2008; 105:5301–6. [PubMed: 18381819]
74. Hagan MF, Chakraborty AK. Hybridization dynamics of surface immobilized DNA. Journal of Chemical Physics. 2004; 120:4958–68. [PubMed: 15267358]
75. Cheng F, Gamble LJ, Castner DG. XPS, TOF-SIMS, NEXAFS, and SPR characterization of nitrilotriacetic acid-terminated self-assembled monolayers for controllable immobilization of proteins. Analytical Chemistry. 2008; 80:2564–73. [PubMed: 18302347]
76. Steven, W.; Metzger, MJL.; Grainger, David W. Surface chemistries enable application of protein microarray technologies to diagnostics. 2002.
77. Dufva M. Fabrication of high quality microarrays. Biomolecular Engineering. 2005; 22:173–84. [PubMed: 16242381]
78. Fielden MR, Halgren RG, Dere E, Zacharewski TR. GP3: GenePix post-processing program for automated analysis of raw microarray data. Bioinformatics. 2002; 18:771–3. [PubMed: 12050078]
79. Dudley AM, Aach J, Steffen MA, Church GM. Measuring absolute expression with microarrays with a calibrated reference sample and an extended signal intensity range. Proc Natl Acad Sci U S A. 2002; 99:7554–9. [PubMed: 12032321]
80. Levicky R, Horgan A. Physicochemical perspectives on DNA microarray and biosensor technologies. Trends in Biotechnology. 2005; 23:143–9. [PubMed: 15734557]
81. Steel AB, Levicky RL, Herne TM, Tarlov MJ. Immobilization of nucleic acids at solid surfaces: Effect of oligonucleotide length on layer assembly. Biophysical Journal. 2000; 79:975–81. [PubMed: 10920027]
82. Seifert JL, Connor RE, Kushon SA, Wang M, Armitage BA. Spontaneous assembly of helical cyanine dye aggregates on DNA nanotemplates. Journal of the American Chemical Society. 1999; 121:2987–95.
83. Randolph JB, Waggoner AS. Stability, specificity and fluorescence brightness of multiply-labeled fluorescent DNA probes. Nucleic Acids Research. 1997; 25:2923–9. [PubMed: 9207044]

84. Allemand JF, Bensimon D, Lavery R, Croquette V. Stretched and overwound DNA forms a Pauling-like structure with exposed bases. Proc Natl Acad Sci U S A. 1998; 95:14152–7. [PubMed: 9826669]

85. Fang X, Li B, Petersen E, Seo YS, Samuilov VA, Chen Y, et al. Drying of DNA droplets. Langmuir. 2006; 22:6308–12. [PubMed: 16800691]

86. Dugas V, Broutin J, Souteyrand E. Droplet evaporation study applied to DNA chip manufacturing. Langmuir. 2005; 21:9130–6. [PubMed: 16171342]

87. Schiessel H, Pincus P. Counterion-condensation-induced collapse of highly charged polyelectrolytes. Macromolecules. 1998; 31:7953–9.

88. Manning GS. The molecular theory of polyelectrolyte solutions with applications to the electrostatic properties of polynucleotides. Quarterly Reviews of Biophysics. 1978; 11:179–246. [PubMed: 353876]

89. Schurr JM, Fujimoto BS. Extensions of counterion condensation theory. I. Alternative geometries and finite salt concentration. Biophysical Chemistry. 2002; 101–102:425–45.

90. Strick TR, Allemand JF, Bensimon D, Croquette V. Behavior of supercoiled DNA. Biophysical Journal. 1998; 74:2016–28. [PubMed: 9545060]

91. Strick TR, Allemand JF, Bensimon D, Bensimon A, Croquette V. The elasticity of a single supercoiled DNA molecule. Science. 1996; 271:1835–7. [PubMed: 8596951]

92. Smith SB, Cui Y, Bustamante C. Overstretching B-DNA: the elastic response of individual double-stranded and single-stranded DNA molecules. Science. 1996; 271:795–9. [PubMed: 8628994]

93. Wang MD, Yin H, Landick R, Gelles J, Block SM. Stretching DNA with optical tweezers. Biophysical Journal. 1997; 72:1335–46. [PubMed: 9138579]

94. Murphy MC, Rasnik I, Cheng W, Lohman TM, Ha T. Probing Single-Stranded DNA Conformational Flexibility Using Fluorescence Spectroscopy. Biophysical Journal. 2004; 86:2530–7. [PubMed: 15041689]

95. Bouchiat C, Wang MD, Allemand JF, Strick T, Block SM, Croquette V. Estimating the persistence length of a worm-like chain molecule from force-extension measurements. Biophysical Journal. 1999; 76:409–13. [PubMed: 9876152]

96. Brinkers S, Dietrich HRC, De Groote FH, Young IT, Rieger B. The persistence length of double stranded DNA determined using dark field tethered particle motion. Journal of Chemical Physics. 2009:130.

97. Bustamante C, Bryant Z, Smith SB. Ten years of tension: Single-molecule DNA mechanics. Nature. 2003; 421:423–7. [PubMed: 12540915]

98. Pardi A, Hare DR, Wang C. Determination of DNA structures by NMR and distance geometry techniques: a computer simulation. Proc Natl Acad Sci U S A. 1988; 85:8785–9. [PubMed: 3194389]

99. Williams, MC.; Maher, LJ. Biophysics of DNA-protein interactions : from single molecules to biological systems. New York: Springer; 2011.

100. Bustamante C, Smith SB, Liphardt J, Smith D. Single-molecule studies of DNA mechanics. Current Opinion in Structural Biology. 2000; 10:279–85. [PubMed: 10851197]

101. Dobrynin AV, Colby RH, Rubinstein M. Scaling theory of polyelectrolyte solutions. Macromolecules. 1995; 28:1859–71.

102. Baumann CG, Smith SB, Bloomfield VA, Bustamante C. Ionic effects on the elasticity of single DNA molecules. Proc Natl Acad Sci U S A. 1997; 94:6185–90. [PubMed: 9177192]

103. Odijk T. Polyelectrolytes near the rod limit. Journal of Polymer Science: Polymer Physics Edition. 1977; 15:477–83.

104. Skolnick J, Fixman M. Electrostatic persistence length of a wormlike polyelectrolyte. Macromolecules. 1977; 10:944–8.

105. Chen H, Meisburger SP, Pabit SA, Sutton JL, Webb WW, Pollack L. Ionic strength-dependent persistence lengths of single-stranded RNA and DNA. Proc Natl Acad Sci U S A. 2012; 109:799–804. [PubMed: 22203973]

106. Savelyev A. Do monovalent mobile ions affect DNA's flexibility at high salt content? Physical Chemistry Chemical Physics. 2012; 14:2250–4. [PubMed: 22246071]

107. Kirste RG. Radius of gyration of stiff chain molecules as a function of the chain length and the interactions with the solvent. Discussions of the Faraday Society. 1970; 49:51–9.
108. Tinland B, Pluen A, Sturm J, Weill G. Persistence length of single-stranded DNA. Macromolecules. 1997; 30:5763–5.
109. Kuznetsov SV, Shen Y, Benight AS, Ansari A. A semiflexible polymer model applied to loop formation in DNA hairpins. Biophysical Journal. 2001; 81:2864–75. [PubMed: 11606297]
110. De Gennes PG. Conformations of polymers attached to an interface. Macromolecules. 1980; 13:1069–75.
111. Halperin A, Buhot A, Zhulina EB. Hybridization at a surface: The role of spacers in DNA microarrays. Langmuir. 2006; 22:11290–304. [PubMed: 17154618]
112. Lehner R, Koota J, Maret G, Gisler T. Segment distributions of end-tethered polymers in a good solvent. Physical review letters. 2006; 96:107801. [PubMed: 16605791]
113. Adamuti-Trache M, McMullen WE, Douglas JF. Segmental concentration profiles of end-tethered polymers with excluded-volume and surface interactions. Journal of Chemical Physics. 1996; 105:4798–811.
114. Rekesh D, Lyubchenko Y, Shlyakhtenko LS, Lindsay SM. Scanning tunneling microscopy of mercapto-hexyl-oligonucleotides attached to gold. Biophysical Journal. 1996; 71:1079–86. [PubMed: 8842244]
115. Mucic RC, Herrlein MK, Mirkin CA, Letsinger RL. Synthesis and characterization of DNA with ferrocenyl groups attached to their 5′-termini: Electrochemical characterization of a redox-active nucleotide monolayer. Chemical Communications. 1996:555–7.
116. Kaiser W, Rant U. Conformations of end-tethered DNA molecules on gold surfaces: influences of applied electric potential, electrolyte screening, and temperature. Journal of the American Chemical Society. 2010; 132:7935–45. [PubMed: 20527934]
117. Schurr JM, Allison SA. Polyelectrolyte contribution to the persistence length of DNA. Biopolymers - Peptide Science Section. 1981; 20:251–68.
118. Schurr JM. Polyanion Models of Nucleic Acid-Metal Ion Interactions. RSC Biomolecular Sciences. 2009:307–49.
119. Manning GS, Ebralidse KK, Mirzabekov AD, Rich A. An estimate of the extent of folding of nucleosomal DNA by laterally asymmetric neutralization of phosphate groups. Journal of Biomolecular Structure and Dynamics. 1989; 6:877–89. [PubMed: 2590506]
120. Savelyev A, Materese CK, Papoian GA. Is DNA's rigidity dominated by electrostatic or nonelectrostatic interactions? Journal of the American Chemical Society. 2011; 133:19290–3. [PubMed: 22039974]
121. Williams LD, Maher LJ Iii. Electrostatic mechanisms of DNA deformation. 2000:497–521.
122. Moulaei T, Maehigashi T, Lountos GT, Komeda S, Watkins D, Stone MP, et al. Structure of B-DNA with cations tethered in the major groove. Biochemistry. 2005; 44:7458–68. [PubMed: 15895989]
123. Vainrub A, Pettitt BM. Coulomb blockage of hybridization in two-dimensional DNA arrays. Physical Review E - Statistical, Nonlinear, and Soft Matter Physics. 2002; 66:041905/1–/4.
124. Nazarenko I, Pires R, Lowe B, Obaidy M, Rashtchian A. Effect of primary and secondary structure of oligodeoxyribonucleotides on the fluorescent properties of conjugated dyes. Nucleic Acids Research. 2002; 30:2089–95. [PubMed: 11972350]
125. Goddard NL, Bonnet G, Krichevsky O, Libchaber A. Sequence dependent rigidity of single stranded DNA. Physical Review Letters. 2000; 85:2400–3. [PubMed: 10978020]
126. Coleman BD, Olson WK, Swigon D. Theory of sequence-dependent DNA elasticity. Journal of Chemical Physics. 2003; 118:7127–40.
127. Dorfman KD, King SB, Olson DW, Thomas JD, Tree DR. Beyond gel electrophoresis: Microfluidic separations, fluorescence burst analysis, and DNA stretching. Chemical Reviews. 2012
128. Moiseev L, Ünlü MS, Swan AK, Goldberg BB, Cantor CR. DNA conformation on surfaces measured by flourescence self-interference. Proc Natl Acad Sci U S A. 2006; 103:2623–8. [PubMed: 16477000]

129. Held G, Grinstein G, Tu Y. Modeling of DNA microarray data by using physical properties of hybridization. Proc Natl Acad Sci U S A. 2003; 100:7575–80. [PubMed: 12808153]
130. Vainrub A, Montgomery Pettitt B. Surface electrostatic effects in oligonucleotide microarrays: control and optimization of binding thermodynamics. Biopolymers. 2003; 68:265–70. [PubMed: 12548628]
131. Wong IY, Melosh NA. An electrostatic model for DNA surface hybridization. Biophysical Journal. 2010; 98:2954–63. [PubMed: 20550908]
132. Shen G, Tercero N, Gaspard MA, Varughese B, Shepard K, Levicky R. Charging behavior of single-stranded DNA polyelectrolyte brushes. Journal of the American Chemical Society. 2006; 128:8427–33. [PubMed: 16802807]
133. Halperin AS, Buhot A, Zhulina EB. Sensitivity, Specificity, and the Hybridization Isotherms of DNA Chips. Biophysical Journal. 2004; 86:718–30. [PubMed: 14747310]
134. Vasiliskov VA, Prokopenko DV, Mirzabekov AD. Parallel multiplex thermodynamic analysis of coaxial base stacking in DNA duplexes by oligodeoxyribonucleotide microchips. Nucleic Acids Research. 2001; 29:2303–13. [PubMed: 11376149]
135. Nguyen TT, Grosberg AY, Shklovskii BI. Screening of a charged particle by multivalent counterions in salty water: strong charge inversion. Journal of Chemical Physics. 2000; 113:1110–25.
136. Vainrub A, Pettitt BM. Thermodynamics of association to a molecule immobilized in an electric double layer. Chemical Physics Letters. 2000; 323:160–6.
137. Netz RR, Andelman D. Neutral and charged polymers at interfaces. Physics Reports. 2003; 380:1–95.
138. Petrovykh DY, Kimura-Suda H, Whitman LJ, Tarlov MJ. Quantitative analysis and characterization of DNA immobilized on gold. Journal of the American Chemical Society. 2003; 125:5219–26. [PubMed: 12708875]
139. Strick T, Allemand JF, Croquette V, Bensimon D. Twisting and stretching single DNA molecules. Progress in Biophysics and Molecular Biology. 2000; 74:115–40. [PubMed: 11106809]
140. Moroz JD, Nelson P. Torsional directed walks, entropic elasticity, and DNA twist stiffness. Proc Natl Acad Sci U S A. 1997; 94:14418–22. [PubMed: 9405627]
141. Zhang J, Lang HP, Yoshikawa G, Gerber C. Optimization of DNA hybridization efficiency by pH-driven nanomechanical bending. Langmuir. 2012; 28:6494–501. [PubMed: 22439593]
142. Marko JF, Siggia ED. Stretching DNA. Macromolecules. 1995; 28:8759–70.
143. Cluzel P, Lebrun A, Heller C, Lavery R, Viovy JL, Chatenay D, et al. DNA: an extensible molecule. Science. 1996; 271:792–4. [PubMed: 8628993]
144. Cloutier TE, Widom J. DNA twisting flexibility and the formation of sharply looped protein-DNA complexes. Proc Natl Acad Sci U S A. 2005; 102:3645–50. [PubMed: 15718281]
145. Forties RA, Bundschuh R, Poirier MG. The flexibility of locally melted DNA. Nucleic Acids Research. 2009; 37:4580–6. [PubMed: 19487242]
146. Cloutier T, Widom J. DNA twisting flexibility and the formation of sharply looped protein–DNA complexes. Proc Natl Acad Sci U S A. 2005; 102:3645–50. [PubMed: 15718281]
147. Zhang Y, Zhou H, Ou-Yang ZC. Stretching single-stranded DNA: Interplay of electrostatic, base-pairing, and base-pair stacking interactions. Biophysical Journal. 2001; 81:1133–43. [PubMed: 11463654]
148. Hansma HG, Kim KJ, Laney DE, Garcia RA, Argaman M, Allen MJ, et al. Properties of biomolecules measured from atomic force microscope images: A review. Journal of Structural Biology. 1997; 119:99–108. [PubMed: 9245749]
149. Bezanilla M, Manne S, Laney DE, Lyubchenko YL, Hansma HG. Adsorption of DNA to mica, silylated mica, and minerals: Characterization by atomic force microscopy. Langmuir. 1995; 11:655–9.
150. Frontali C, Dore E, Ferrauto A, Gratton E, Bettini A, Pozzan MR, et al. An absolute method for the determination of the persistence length of native DNA from electron micrographs. Biopolymers - Peptide Science Section. 1979; 18:1353–73.

151. Hagerman PJ. Flexibility of DNA. Annual review of biophysics and biophysical chemistry. 1988; 17:265–86.
152. Protozanova E, Yakovchuk P, Frank-Kamenetskii MD. Stacked-unstacked equilibrium at the nick site of DNA. Journal of Molecular Biology. 2004; 342:775–85. [PubMed: 15342236]
153. Caserta M, Agricola E, Churcher M, Hiriart E, Verdone L, Di mauro E, et al. A translational signature for nucleosome positioning in vivo. Nucleic Acids Research. 2009; 37:5309–21. [PubMed: 19596807]
154. Morriss-Andrews A, Rottler J, Plotkin SS. A systematically coarse-grained model for DNA and its predictions for persistence length, stacking, twist, and chirality. Journal of Chemical Physics. 2010:132.
155. Ambia-Garrido J, Vainrub A, Pettitt BM. A model for structure and thermodynamics of ssDNA and dsDNA near a surface: A coarse grained approach. Computer Physics Communications. 2010; 181:2001–7. [PubMed: 20957064]
156. Rechendorff K, Witz G, Adamcik J, Dietler G. Persistence length and scaling properties of single-stranded DNA adsorbed on modified graphite. Journal of Chemical Physics. 2009:131.
157. Crozier PS, Stevens MJ. Simulations of single grafted polyelectrolyte chains: ssDNA and dsDNA. Journal of Chemical Physics. 2003; 118:3855–60.
158. Erts D, Polyakov B, Olin H, Tuite E. Spatial and mechanical properties of dilute DNA monolayers on gold imaged by AFM. Journal of Physical Chemistry B. 2003; 107:3591–7.
159. Levicky R, Herne TM, Tarlov MJ, Satija SK. Using self-assembly to control the structure of DNA monolayers on gold: A neutron reflectivity study. Journal of the American Chemical Society. 1998; 120:9787–92.
160. Wang J, Rivas G, Cai X, Chicharro M, Parrado C, Dontha N, et al. Detection of point mutation in the p53 gene using peptide nucleic acid biosensor. Analytica Chimica Acta. 1997; 344:111–8.
161. Abels JA, Moreno-Herrero F, Van Der Heijden T, Dekker C, Dekker NH. Single-molecule measurements of the persistence length of double-stranded. RNA Biophysical Journal. 2005; 88:2737–44.
162. Mastroianni AJ, Sivak DA, Geissler PL, Alivisatos AP. Probing the conformational distributions of subpersistence length DNA. Biophysical Journal. 2009; 97:1408–17. [PubMed: 19720029]
163. Bryant Z, Stone MD, Gore J, Smith SB, Cozzarelli NR, Bustamante C. Structural transitions and elasticity from torque measurements on DNA. Nature. 2003; 424:338–41. [PubMed: 12867987]
164. Kratky O, Porod G. Diffuse small-angle scattering of x-rays in colloid systems. Journal of Colloid Science. 1949; 4:35–70. [PubMed: 18110601]
165. Rippe K, Von Hippel PH, Langowski J. Action at a distance: DNA-looping and initiation of transcription. Trends in Biochemical Sciences. 1995; 20:500–6. [PubMed: 8571451]
166. Shimada J, Yamakawa H. Ring-closure probabilities for twisted wormlike chains. Application to DNA. Macromolecules. 1984; 17:689–98.
167. Maddox J. The case for a great many journals. Nature. 1995; 375:11. [PubMed: 7723830]
168. Bensimon D, Simon AJ, Croquette VV, Bensimon A. Stretching DNA with a receding meniscus: Experiments and models. Physical review letters. 1995; 74:4754–7. [PubMed: 10058590]
169. Van mameren J, Peterman EJG, Wuite GJL. See me, feel me: Methods to concurrently visualize and manipulate single DNA molecules and associated proteins. Nucleic Acids Research. 2008; 36:4381–9. [PubMed: 18586820]
170. Seol Y, Li J, Nelson PC, Perkins TT, Betterton MD. Elasticity of short DNA molecules: Theory and experiment for contour lengths of 0.6–7 μm. Biophysical Journal. 2007; 93:4360–73. [PubMed: 17766363]
171. Wiggins PA, Nelson PC. Generalized theory of semiflexible polymers. Physical Review E - Statistical, Nonlinear, and Soft Matter Physics. 2006:73.
172. Rant U, Arinaga K, Scherer S, Pringsheim E, Fujita S, Yokoyama N, et al. Switchable DNA interfaces for the highly sensitive detection of label-free DNA targets. Proc Natl Acad Sci U S A. 2007; 104:17364–9. [PubMed: 17951434]
173. Biophysics: DNA is as elastic as nylon. Nature. 2011; 477:372.

174. Van Eijck L, Merzel F, Rols S, Ollivier J, Forsyth VT, Johnson MR. Direct determination of the base-pair force constant of DNA from the acoustic phonon dispersion of the double helix. Physical review letters. 2011:107.
175. Morii T, Mizuno R, Haruta H, Okada T. An AFM study of the elasticity of DNA molecules. Thin Solid Films. 2004; 464–465:456–8.
176. Nelson P. New measurements of DNA twist elasticity. Biophysical Journal. 1998; 74:2501–3. [PubMed: 9591676]
177. Marko JF. Stretching must twist DNA. Europhysics Letters. 1997; 38:183–8.
178. Stasiak A, Di Capua E. The helicity of DNA in complexes with RecA protein. Nature. 1982; 299:185–6. [PubMed: 7050731]
179. Léger JF, Romano G, Sarkar A, Robert J, Bourdieu L, Chatenay D, et al. Structural transitions of a twisted and stretched DNA molecule. Physical review letters. 1999; 83:1066–9.
180. Sarkar A, Léger JF, Chatenay D, Marko JF. Structural transitions in DNA driven by external force and torque. Physical Review E - Statistical, Nonlinear, and Soft Matter Physics. 2001; 63:519031–5190310.
181. Wenner JR, Williams MC, Rouzina I, Bloomfield VA. Salt dependence of the elasticity and overstretching transition of single DNA molecules. Biophysical Journal. 2002; 82:3160–9. [PubMed: 12023240]
182. Punkkinen O, Hansen PL, Miao L, Vattulainen I. DNA overstretching transition: Ionic strength effects. Biophysical Journal. 2005; 89:967–78. [PubMed: 15923227]
183. Le Bret M, Zimm BH. Monte Carlo determination of the distribution of ions about a cylindrical polyelectrolyte. Biopolymers - Peptide Science Section. 1984; 23:271–85.
184. Williams MC, Wenner JR, Rouzina I, Bloomfield VA. Effect of pH on the overstretching transition of double-stranded DNA: Evidence of force-induced DNA melting. Biophysical Journal. 2001; 80:874–81. [PubMed: 11159454]
185. Kamien RD, Lubensky TC, Nelson P, O'Hern CS. Direct determination of DNA twist-stretch coupling. Europhysics Letters. 1997; 38:237–42.
186. Gore J, Bryant Z, Nöllmann M, Le MU, Cozzarelli NR, Bustamante C. DNA overwinds when stretched. Nature. 2006; 442:836–9. [PubMed: 16862122]
187. Raghunathan, K.; Chenc, YF.; Blaty, J.; Juliar, BA.; Milstein, J.; Meiners, JC. Mechanics of DNA: Sequence dependent elasticity. San Diego, CA: 2011.
188. Sheinin MY, Forth S, Marko JF, Wang MD. Underwound DNA under tension: Structure, elasticity, and sequence-dependent behaviors. Physical review letters. 2011:107.
189. Yang Z, Haijun Z, Zhong-Can OY. Monte Carlo implementation of supercoiled double-stranded DNA. Biophysical Journal. 2000; 78:1979–87. [PubMed: 10733976]
190. Hansma HG, Laney DE, Bezanilla M, Sinsheimer RL, Hansma PK. Applications for atomic force microscopy of DNA. Biophysical Journal. 1995; 68:1672–7. [PubMed: 7612809]
191. Gao L, Wu J, Gao D, Wu J. Separation of long DNA molecules through cleavage of hydrogen bonds under a stretching force. Applied Physics Letters. 2007:91.
192. Gray DE, Case-Green SC, Fell TS, Dobson PJ, Southern EM. Ellipsometric and interferometric characterization of DNA probes immobilized on a combinatorial array. Langmuir. 1997; 13:2833–42.
193. Chrisey LA, O'Ferrall CE, Spargo BJ, Dulcey CS, Calvert JM. Fabrication of patterned DNA surfaces. Nucleic Acids Research. 1996; 24:3040–7. [PubMed: 8760891]
194. Levicky R, Koneripalli N, Tirrell M, Satija SK. Stratification in bidisperse polymer brushes from neutron reflectivity. Macromolecules. 1998; 31:2616–21.
195. Herne TM, Tarlov MJ. Characterization of DNA probes immobilized on gold surfaces. Journal of the American Chemical Society. 1997; 119:8916–20.
196. Peterlinz KA, Georgiadis RM, Herne TM, Tarlov MJ. Observation of hybridization and dehybridization of thiol-tethered DNA using two-color surface plasmon resonance spectroscopy. Journal of the American Chemical Society. 1997; 119:3401–2.
197. Kelley SO, Barton JK, Jackson NM, McPherson LD, Potter AB, Spain EM, et al. Orienting DNA helices on gold using applied electric fields. Langmuir. 1998; 14:6781–4.

198. Rant U, Arinaga K, Tornow M, Yong WK, Netz RR, Fujita S, et al. Dissimilar kinetic behavior of electrically manipulated single- and double-stranded DNA tethered to a gold surface. Biophysical Journal. 2006; 90:3666–71. [PubMed: 16473909]

199. Edman CF, Raymond DE, Wu DJ, Tu E, Sosnowski RG, Butler WF, et al. Electric field directed nucleic acid hybridization on microchips. Nucleic Acids Research. 1997; 25:4907–14. [PubMed: 9396795]

200. Steel AB, Herne TM, Tarlov MJ. Electrochemical quantitation of DNA immobilized on gold. Analytical Chemistry. 1998; 70:4670–7. [PubMed: 9844566]

201. Fritz J, Cooper EB, Gaudet S, Sorger PK, Manalis SR. Electronic detection of DNA by its intrinsic molecular charge. Proc Natl Acad Sci U S A. 2002; 99:14142–6. [PubMed: 12386345]

202. Heaton RJ, Peterson AW, Georgiadis RM. Electrostatic surface plasmon resonance: direct electric field-induced hybridization and denaturation in monolayer nucleic acid films and label-free discrimination of base mismatches. Proc Natl Acad Sci U S A. 2001; 98:3701–4. [PubMed: 11259682]

203. Bhanot G, Louzoun Y, Zhu J, DeLisi C. The importance of thermodynamic equilibrium for high throughput gene expression arrays. Biophysical Journal. 2003; 84:124–35. [PubMed: 12524270]

204. Bishop J, Chagovetz A, Blair S. Kinetics of multiplex hybridization: mechanisms and implications. Biophysical Journal. 2008; 94:1726–34. [PubMed: 17993490]

205. Henry MR, Wilkins Stevens P, Sun J, Kelso DM. Real-time measurements of DNA hybridization on microparticles with fluorescence resonance energy transfer. Analytical Biochemistry. 1999; 276:204–14. [PubMed: 10603244]

206. Guo Z, Guilfoyle RA, Thiel AJ, Wang R, Smith LM. Direct fluorescence analysis of genetic polymorphisms by hybridization with oligonucleotide arrays on glass supports. Nucleic Acids Research. 1994; 22:5456–65. [PubMed: 7816638]

207. Su HJ, Surrey S, McKenzie SE, Fortina P, Graves DJ. Kinetics of heterogeneous hybridization on indium tin oxide surfaces with and without an applied potential. Electrophoresis. 2002; 23:1551–7. [PubMed: 12116168]

208. Dimitrov RA, Zuker M. Prediction of hybridization and melting for double-stranded nucleic acids. Biophysical Journal. 2004; 87:215–26. [PubMed: 15240459]

209. Hassibi A, Vikalo H, Riechmann JL, Hassibi B. Real-time DNA microarray analysis. Nucleic Acids Res. 2009:37.

210. Toegl A, Kirchner R, Gauer C, Wixforth A. Enhancing results of microarray hybridizations through microagitation. J Biomol Tech. 2003; 14:197–204. [PubMed: 13678150]

211. Chagovetz A, Blair S. Real-time DNA microarrays: reality check. Biochemical Society Transactions. 2009; 37:471. [PubMed: 19290884]

212. Walter J-C, Kroll KM, Hooyberghs J, Carlon E. Nonequilibrium effects in DNA microarrays: a multiplatform study. The Journal of Physical Chemistry B. 2011; 115:6732–9. [PubMed: 21542593]

213. Carletti E, Guerra E, Alberti S. The forgotten variables of DNA array hybridization. Trends Biotechnol. 2006; 24:443–8. [PubMed: 16904784]

214. Horne M, Fish D, Benight A. Statistical thermodynamics and kinetics of DNA multiplex hybridization reactions. Biophysical Journal. 2006; 91:4133–53. [PubMed: 16963510]

215. Chen C, Wang W, Ge J, Zhao XS. Kinetics and thermodynamics of DNA hybridization on gold nanoparticles. Nucleic Acids Research. 2009; 37:3756–65. [PubMed: 19380378]

216. Forman, JE.; Walton, ID.; Stern, D.; Rava, RP.; Trulson, MO. Thermodynamics of Duplex Formation and Mismatch Discrimination on Photolithographically Synthesized Oligonucleotide Arrays. 1998. p. 206-28.

217. Naef F, Magnasco MO. Solving the riddle of the bright mismatches: Labeling and effective binding in oligonucleotide arrays. Physical Review E - Statistical, Nonlinear, and Soft Matter Physics. 2003; 68:119061–4.

218. Erickson D, Liu X, Krull U, Li D. Electrokinetically controlled DNA hybridization microfluidic chip enabling rapid target analysis. Analytical Chemistry. 2004; 76:7269–77. [PubMed: 15595869]

219. Unruh JR, Gokulrangan G, Lushington GH, Johnson CK, Wilson GS. Orientational dynamics and dye-DNA interactions in a dye-labeled DNA aptamer. Biophysical Journal. 2005; 88:3455–65. [PubMed: 15731389]
220. Hermanson, GT. Bioconjugate Techniques. Academic Press, Elsevier; 2008.
221. Beaucage SL. Strategies in the preparation of DNA oligonucleotide arrays for diagnostic applications. Current Medicinal Chemistry. 2001; 8:1213–44. [PubMed: 11472237]
222. Gao Y, Wolf LK, Georgiadis RM. Secondary structure effects on DNA hybridization kinetics: A solution versus surface comparison. Nucleic Acids Research. 2006; 34:3370–7. [PubMed: 16822858]
223. Nguyen TH, Hilton JP, Lin Q. Emerging applications of aptamers to micro- and nanoscale biosensing. Microfluidics and Nanofluidics. 2009; 6:347–62.
224. Drake TJ, Tan W. Molecular Beacon DNA Probes and their Bioanalytical Applications. Applied Spectroscopy. 2004; 58:269A–80A.
225. Di Giusto DA, Wlassoff WA, Gooding JJ, Messerle BA, King GC. Proximity extension of circular DNA aptamers with real-time protein detection. Nucleic Acids Research. 2005; 33:e64–e. [PubMed: 15817563]
226. Wang K, Tang Z, Yang CJ, Kim Y, Fang X, Li W, et al. Molecular engineering of DNA: molecular beacons. Angewandte Chemie - International Edition. 2009; 48:856–70.
227. Fang X, Liu X, Schuster S, Tan W. Designing a novel molecular beacon for surface-immobilized DNA hybridization studies. Journal of the American Chemical Society. 1999; 121:2921–2.
228. Tan W, Wang K, Drake TJ. Molecular beacons. Current opinion in chemical biology. 2004; 8:547–53. [PubMed: 15450499]
229. SantaLucia J Jr, Hicks D. The thermodynamics of DNA structural motifs. Annual review of biophysics and biomolecular structure. 2004; 33:415–40.
230. Wang H, Li J, Liu H, Liu Q, Mei Q, Wang Y, et al. Label-free hybridization detection of a single nucleotide mismatch by immobilization of molecular beacons on an agarose film. Nucleic Acids Research. 2002; 30:e61–e. [PubMed: 12060699]
231. Marras SA, Tyagi S, Kramer FR. Real-time assays with molecular beacons and other fluorescent nucleic acid hybridization probes. Clinica Chimica Acta. 2006; 363:48–60.
232. Du H, Strohsahl CM, Camera J, Miller BL, Krauss TD. Sensitivity and specificity of metal surface-immobilized “molecular beacon” biosensors. Journal of the American Chemical Society. 2005; 127:7932–40. [PubMed: 15913384]
233. Bonnet G, Tyagi S, Libchaber A, Kramer FR. Thermodynamic basis of the enhanced specificity of structured DNA probes. Proc Natl Acad Sci U S A. 1999; 96:6171–6. [PubMed: 10339560]
234. Yao G, Fang X, Yokota H, Yanagida T, Tan W. Monitoring molecular beacon DNA probe hybridization at the single-molecule level. Chemistry-A European Journal. 2003; 9:5686–92.
235. Aalberts DP, Parman JM, Goddard NL. Single-strand stacking free energy from DNA beacon kinetics. Biophysical Journal. 2003; 84:3212–7. [PubMed: 12719250]
236. Jung J, Van Orden A. Folding and unfolding kinetics of DNA hairpins in flowing solution by multiparameter fluorescence correlation spectroscopy. The Journal of Physical Chemistry B. 2005; 109:3648–57. [PubMed: 16851403]
237. Kastantin M, Schwartz DK. DNA Hairpin Stabilization on a Hydrophobic Surface. Small. 2012
238. Perelaer J, Smith PJ, Wijnen MMP, Van Den Bosch E, Eckardt R, Ketelaars PHJM, et al. Droplet tailoring using evaporative inkjet printing. Macromolecular Chemistry and Physics. 2009; 210:387–93.
239. Hu H, Larson RG. Marangoni effect reverses coffee-ring depositions. Journal of Physical Chemistry B. 2006; 110:7090–4.
240. Bietsch A, Hegner M, Lang HP, Gerber C. Inkjet deposition of alkanethiolate monolayers and DNA oligonucleotides on gold: Evaluation of spot uniformity by wet etching. Langmuir. 2004; 20:5119–22. [PubMed: 15984277]
241. Deegan RD, Bakajin O, Dupont TF, Huber G, Nagel SR, Witten TA. Capillary flow as the cause of ring stains from dried liquid drops. Nature. 1997; 389:827–9.

242. Yunker PJ, Still T, Lohr MA, Yodh AG. Suppression of the coffee-ring effect by shape-dependent capillary interactions. Nature. 2011; 476:308–11. [PubMed: 21850105]

243. Weon BM, Je JH. Capillary force repels coffee-ring effect. Physical Review E - Statistical, Nonlinear, and Soft Matter Physics. 2010:82.

244. Poulard C, Damman P. Control of spreading and drying of a polymer solution from Marangoni flows. EPL (Europhysics Letters). 2007; 80:64001.

245. Gong P, Harbers GM, Grainger DW. Multi-technique comparison of immobilized and hybridized oligonucleotide surface density on commercial amine-reactive microarray slides. Analytical Chemistry. 2006; 78:2342–51. [PubMed: 16579618]

246. Lee CY, Harbers GM, Grainger DW, Gamble LJ, Castner DG. Fluorescence, XPS, and TOF-SIMS surface chemical state image analysis of DNA microarrays. Journal of the American Chemical Society. 2007; 129:9429–38. [PubMed: 17625851]

247. Pappaert K, Ottevaere H, Thienpont H, Van Hummelen P, Desmet G. Diffusion limitation: A possible source for the occurrence of doughnut patterns on DNA microarrays. BioTechniques. 2006; 41:609–16. [PubMed: 17140119]

248. McQuain MK, Seale K, Peek J, Levy S, Haselton FR. Effects of relative humidity and buffer additives on the contact printing of microarrays by quill pins. Analytical Biochemistry. 2003; 320:281–91. [PubMed: 12927835]

249. Still T, Yunker PJ, Yodh AG. Surfactant-induced Marangoni eddies alter the coffee-rings of evaporating colloidal drops. Langmuir. 2012; 28:4984–8. [PubMed: 22369657]

250. Smalyukh II, Zribi OV, Butler JC, Lavrentovich OD, Wong GCL. Structure and dynamics of liquid crystalline pattern formation in drying droplets of DNA. Physical review letters. 2006; 96:177801. [PubMed: 16712331]

251. Kaya D, Belyi V, Muthukumar M. Pattern formation in drying droplets of polyelectrolyte and salt. The Journal of chemical physics. 2010; 133:114905. [PubMed: 20866155]

252. Truskett VN, Stebe KJ. Influence of surfactants on an evaporating drop: Fluorescence images and particle deposition patterns. Langmuir. 2003; 19:8271–9.

253. Lee K, Ivanova N, Starov V, Hilal N, Dutschk V. Kinetics of wetting and spreading by aqueous surfactant solutions. Advances in colloid and interface science. 2008; 144:54–65. [PubMed: 18834966]

254. Dias R, Rosa M, Pais AC, Miguel M, Lindman B. DNA-surfactant interactions. Compaction, condensation, decompaction and phase separation. JOURNAL-CHINESE CHEMICAL SOCIETY TAIPEI. 2004; 51:447–70.

255. Zanchetta G, Nakata M, Buscaglia M, Bellini T, Clark NA. Phase separation and liquid crystallization of complementary sequences in mixtures of nanoDNA oligomers. Proceedings of the National Academy of Sciences. 2008; 105:1111.

256. Liu F, Yang J, Huang L, Liu D. Effect of Non-Ionic Surfactants on the Formation of DNA/Emulsion Complexes and Emulsion-Mediated Gene Transfer. Pharmaceutical Research. 1996; 13:1642–6. [PubMed: 8956328]

257. Armitage BA. Cyanine dye–DNA interactions: intercalation, groove binding, and aggregation. DNA Binders and Related Subjects. 2005:55–76.

258. Ogul'chansky TY, Losytskyy MY, Kovalska V, Yashchuk V, Yarmoluk S. Interactions of cyanine dyes with nucleic acids. XXIV. Aggregation of monomethine cyanine dyes in presence of DNA and its manifestation in absorption and fluorescence spectra. Spectrochimica Acta Part A: Molecular and Biomolecular Spectroscopy. 2001; 57:1525–32.

259. Lehmann U. Aggregation of cyanine dyes at Langmuir-Blodgett monolayers. Thin Solid Films. 1988; 160:257–69.

260. Eral HB, Augustine DM, Duits MHG, Mugele F. Suppressing the coffee stain effect: How to control colloidal self-assembly in evaporating drops using electrowetting. Soft Matter. 2011; 7:4954–8.

261. Moran-Mirabal JM, Tan CP, Orth RN, Williams EO, Craighead HG, Lin DM. Controlling microarray spot morphology with polymer liftoff arrays. Analytical Chemistry. 2007; 79:1109–14. [PubMed: 17263343]

262. Oh JM, Legendre D, Mugele F. Shaken not stirred - On internal flow patterns in oscillating sessile drops. Europhysics Letters. 2012:98.

263. Larson RG. Re-shaping the coffee ring. Angewandte Chemie - International Edition. 2012; 51:2546–8.

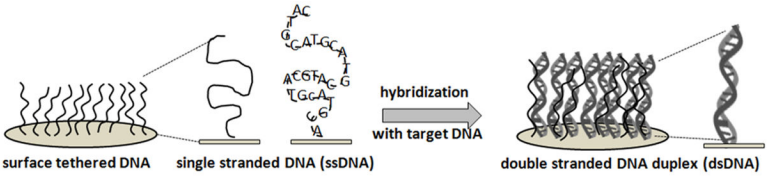

Figure 1.

Single-strand DNA-probe immobilization in tethered “brush” formats (left), and double strand target hybridization at surfaces (right): the working principle for DNA microarrays as surface-capture assays.

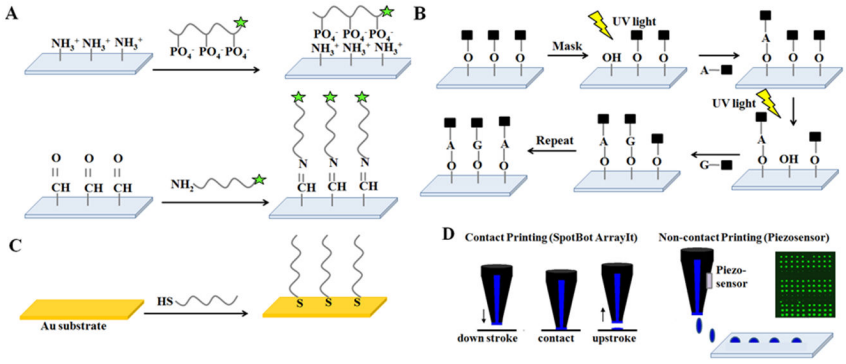

Figure 2.

General methods to fabricate DNA arrays. A) “Grafting to”: probe DNA surface immobilization by electrostatic interactions: DNA binding to amine-derivatized surfaces by ionic interactions between cationic primary amine surface groups and anionic DNA phosphate groups. Alternatively, covalent “grafting to”: probe DNA immobilization by Schiff’s base reactions using amine-modified DNA and aldehyde-derivatized surfaces. Other amine-reactive chemistries are also popular. B) “Grafting from”: photochemical, spatially controlled (e.g., Affymetrix Genechip™, NimbleGen) probe fabrication by *in situ* synthesis using sequential photoactivation and deprotection of nucleic acids. Photomask or maskless UV irradiation over localized surface regions selectively activates nucleotides that react with growing chains ends on surfaces, producing patterned arrays with pre-determined DNA chain chemical diversity, and at high density. C) “Grafting to” using chemisorption of thiolated DNA probe oligomers on coinage metal substrates via metal-thiolate bonds. D) Micro/nano droplet contact and non-contact (e.g., piezo) printing of DNA probe solutions in defined array patterns, with subsequent droplet drying and immobilization by both physical and chemical reactions with surfaces.

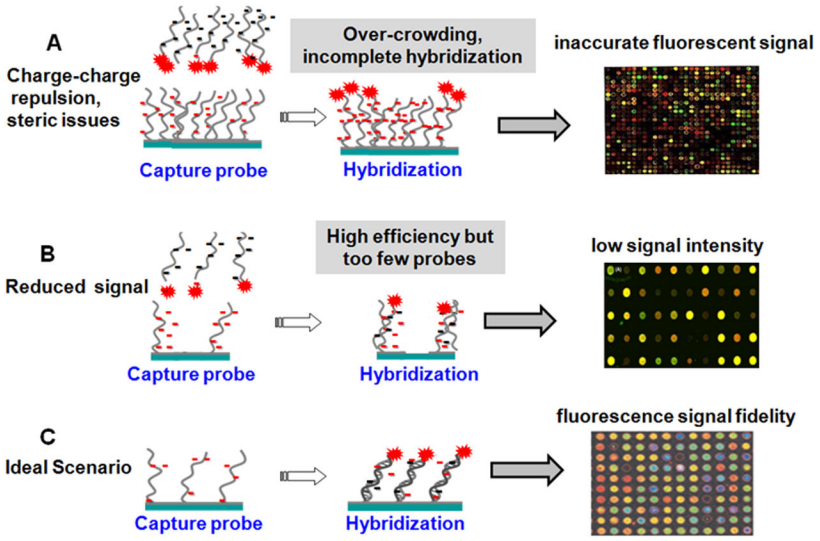

Figure 3.

The DNA probe surface density challenge and the Goldilocks principle of surface tethering optimization: A) High density of immobilized DNA oligomer probes presents both steric and electrostatic barriers that preclude accurate target capture and alter hybridization kinetics. B) Low immobilized probe densities capture target at high efficiency but the end result is often insufficient assay signal and high background noise from non-specific surface capture. C) Optimal probe density, while such optimization is case dependent on probe sequence and length and surface assay conditions, might be described as a condition between these two extremes in (A) and (B) where sufficient assay signal is produced at reasonable time scales and with fidelity to both target abundance and sequence.

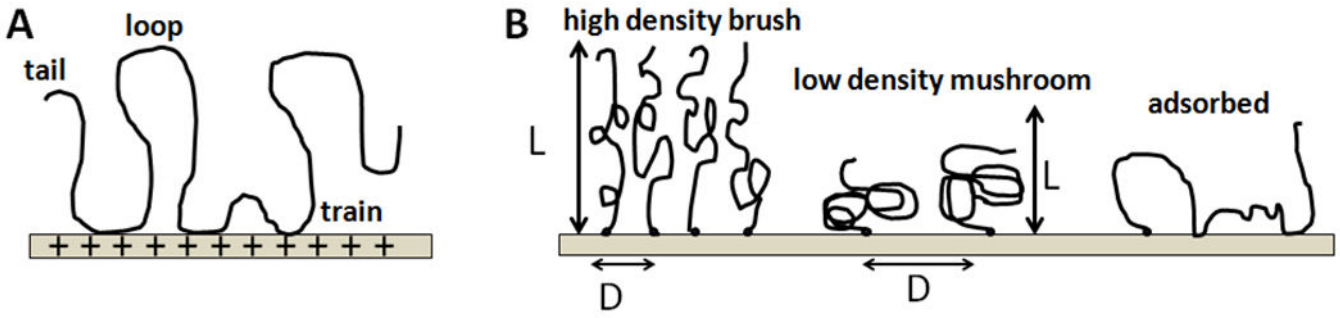

Figure 4.

Schematics of DNA chain adsorbed-state conformations on surfaces. A) Multivalent interactions of a single DNA chain with the substrate leading to tail, loop and train sections of the adsorbed chain; B) Surface-tethered DNA chains can form either “mushroom”-like or “brush”-like molecular conformations, depending on surface grafting density. At very low grafting density, the DNA chain lies roughly flat on the surface with multiple binding behaviors unless displaced by surface-binding diluents.

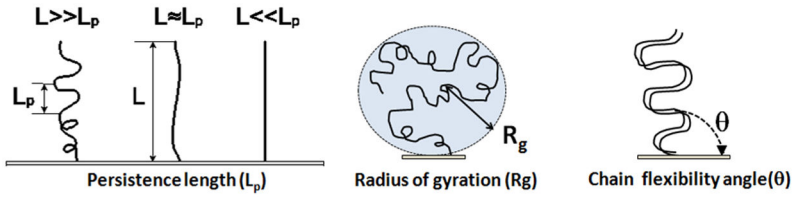

Figure 5.

Persistence length, radius of gyration and chain flexibility angle for immobilized ssDNA and dsDNA tethered ideally on surfaces.

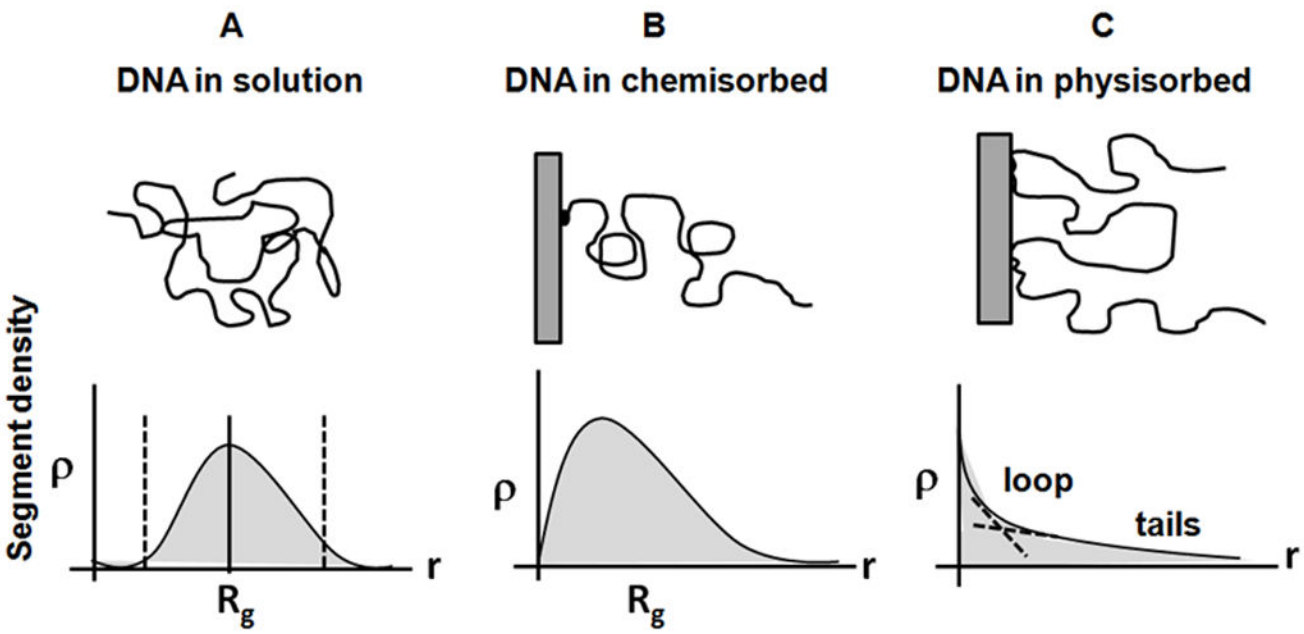

Figure 6.

Schematics of DNA segment distribution as a function of distance from the surface. A) DNA in solution. B) DNA chemisorbed (end-tethered) on a surface, and C) DNA physisorbed on a surface, forming tails, loops and trains (see Fig. 3).

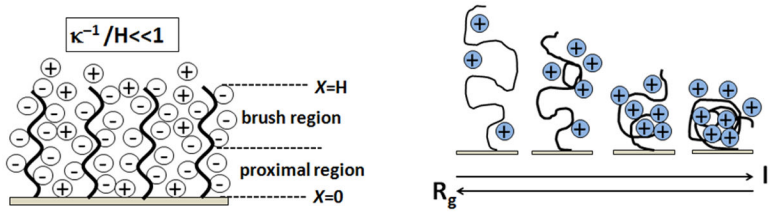

Figure 7.

Surface coulombic blockage of target DNA by immobilized ssDNA (polyanion theory) due to DNA nucleotide phosphate anions and their Debye length dependence (κ^{-1}) (left), and the effect of increasing ionic strength (I) on the DNA polyanion radius of gyration (R_g) (right).

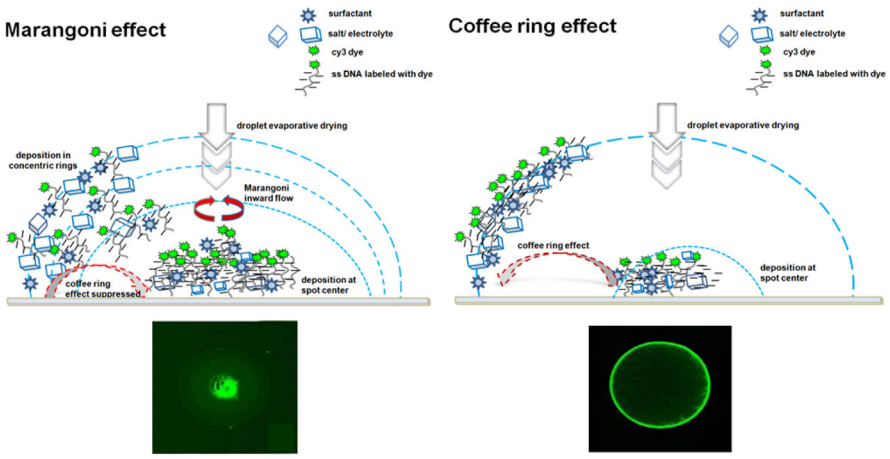

Figure 8.

Schematics of DNA droplet drying phenomena: Marangoni (left) vs. coffee ring effect (right) for printed spots. Actual fluorescent images of these respective effects on individual printed, dried array spots are shown below each depiction.

Table 1

Important technical considerations for improving the design and development of nucleic acid microarrays

Microarray methods	Major challenges	References
Microarray design	Addressing the biological question with selection of proper controls, fiduciary markers, internal calibrations, quality controls	[26, 266, 267]
Experimental processing	Probe immobilization, target preparation from complex milieu and reliable hybridization, sample-to-answer time efficiencies, signal: noise challenges	[1, 17, 21]
Data extraction	Assay (e.g., fluorescence) signal translation for quantification of gene of interest, absolute abundance correlations, reliable quantitation, platform-platform correlation	[268–271]
Data analysis and modeling	Standardized, validated bioinformatics and biostatistics algorithms	[272–274]
Data repeatability and reproducibility	MAQC-I, -II and -III-identified optimization, reliability, intra- and inter-platform reproducibility issues	[13, 275, 276]
Limited database access	Access to web-based data-mining platforms aimed at facilitating discovery from genome- wide expression analyses	[10, 277, 278]

Table 2

DNA feature sizes and probe densities for the various array fabrication methods

Surface	Area	Probe density/cm^2
Gold	100 μm diameter spot	5×10^{12}
Amine-modified surface	4.5mm diameter spot	2.5×10^{12}
Photolithography	5–10 μm	10^6

Table 3

Comparison of actual ssDNA conditions experienced at array surfaces versus those typically reported in ssDNA physicochemical models and simulations.

ssDNA properties at surfaces	**ssDNA tethered in microarrays**	**ssDNA brush modeling**
ssDNA grafting density	Uncontrolled grafting density, spanning sparse, mushroom and brush in the same surface locale	Controlled, uniform grafting density of mushroom or brush across an impenetrable surface
Tethered ssDNA chain orientations	Uncontrolled immobilized chain orientations and conformations	Uniform controlled brush heights and chain orientations
ssDNA chain lengths	20–200 bases (short) probes	>1000 bases (long) brushes
ssDNA chain flexibility	ssDNA is short, rigid, rod-like	ssDNA is longer, flexlble
ssDNA solvent/media exposure	High ionic strength but complex mixed salt solutions, surfactants and other solutes in drying cycles	Wide range of salt concentrations (monovalent)
Interactive conditions at the surface	Repeated surface solvation/drying steps in assay that modulate ionic strength and solvation dramatically	Equilibrium models or constrained simulations, with little dynamic interactive changes in polymer/solvent/surface conditions
ssDNA chain dynamics under a given analysis	Persistence lengths, radius of gyration, brush heights and chain condensation vary widely	Persistence lengths, radius of gyration, brush heights and chain condensation vary little